Phase-field-crystal dynamics for binary systems: Derivation from dynamical density functional theory, amplitude equation formalism, and applications to alloy heterostructures

Zhi-Feng Huang
Department of Physics and Astronomy, Wayne State University, Detroit, Michigan 48201, USA

K. R. Elder
Department of Physics, Oakland University, Rochester, Michigan 48309, USA

Nikolas Provatas
Department of Materials Science and Engineering and Brockhouse Institute for Materials Research, McMaster University, Hamilton, Ontario, Canada L8S-4L7

(Received 7 June 2010; published 19 August 2010)

The dynamics of phase field crystal (PFC) modeling is derived from dynamical density functional theory (DDFT), for both single-component and binary systems. The derivation is based on a truncation up to the three-point direct correlation functions in DDFT, and the lowest order approximation using scale analysis. The complete amplitude equation formalism for binary PFC is developed to describe the coupled dynamics of slowly varying complex amplitudes of structural profile, zeroth-mode average atomic density, and system concentration field. Effects of noise (corresponding to stochastic amplitude equations) and species-dependent atomic mobilities are also incorporated in this formalism. Results of a sample application to the study of surface segregation and interface intermixing in alloy heterostructures and strained layer growth are presented, showing the effects of different atomic sizes and mobilities of alloy components. A phenomenon of composition overshooting at the interface is found, which can be connected to the surface segregation and enrichment of one of the atomic components observed in recent experiments of alloying heterostructures.

DOI: 10.1103/PhysRevE.82.021605 PACS number(s): 81.10.Aj, 05.70.Ln, 81.15.Aa, 64.60.My

I. INTRODUCTION

Understanding the formation and dynamics of complex spatial structures or patterns has been of continuing interest due to the fundamental importance of predicting and controlling system properties and material functions. However, a comprehensive understanding is hindered by the fact that the processes involved are usually nonlinear, nonequilibrium, can span a variety of length and time scales, and are highly influenced by the complex coupling with materials growth and processing conditions. Typical examples include the growth of strained solid films and the formation of nanostructures such as quantum dots or nanowires, which involve the interplay among microscopic crystalline structure, mesoscopic, or nanoscale surface pattern, topological defects (e.g., dislocations), as well as various growth parameters such as temperature, misfit strain, growth rate, and film thickness [1–3]. The system dynamics and evolution are further complicated in alloy samples, due to the additional coupling to spatial/temporal variation of alloy composition particularly in the case of phase separation [4,5].

To address these complex phenomena a variety of theoretical modeling and simulation methods have been developed, which can be roughly characterized via the level of description that they focus on. At the microscopic level capturing crystalline details, atomistic modeling techniques such as Monte Carlo (MC) or molecular dynamics (MD) have been widely adopted. For example, nanostructure (e.g., islands/pits) formation during strained film epitaxy has been studied via the kinetic MC method incorporating elastic interaction and strain energy [6–8], while detailed structure and dynamics of crystal defects like grain boundaries and dislocations have been simulated by MD [9,10]. However, the limitation of small length and time scales addressed in these atomistic methods leads to large computational demands and hence the restriction of system size and evolution time range that can be accessed. Such limitation can be overcome via continuum modeling methods, including continuum elasticity theory used in strained film growth [5,11–17] and the well-known phase field models that have been applied to a wide range of areas such as crystal growth, nucleation, phase separation, solidification, defect dynamics, etc. [18–22]. These continuum approaches feature coarse-grained, long-wavelength scales and diffusive time dynamics, but are not formulated for the short-wavelength scales associated with microscopic crystalline details.

To incorporate the advantages of these approaches and hence be able to simultaneously model crystalline details on length and time scales of experimental relevance, the phase field crystal (PFC) [23–25] model and the related amplitude representation [26–30] were developed recently. The PFC model incorporates the small length scales of the crystalline structure with diffusive time scales by describing the dynamics of the atomic number density field ρ, a continuum field variable that is spatially periodic at atomic length scales in crystalline state [23,24]. To alleviate the limitation imposed by the necessity of describing small length scales, an amplitude representation was developed to describe slowly varying envelope or amplitude functions while maintaining the basic features of crystalline states, particularly elasticity, plasticity and multiple crystal orientations. Both the original PFC and corresponding amplitude representation have been

 ©2010 The American Physical Society

extended to binary alloys [25,31,32]. In the binary case the amplitude representation describes the amplitude and phase of the density field [26–28,30] and also the concentration profile [32], which is assumed to vary on "slow" scales compared to atomic lattice spacing. A wide range of phenomena has been studied via this PFC method for both pure and binary material systems, including solidification [25,32,33], grain nucleation and growth [26,30,34,35], phase segregation [25,32], quantum dot growth during epitaxy [3,32,36,37], surface energy anisotropy [38,39], formation and melting of dislocations and grain boundaries [40–43], commensurate/incommensurate transitions [44,45], sliding friction [46,47], and glass formation [48]. In addition, recent work has been conducted to extend the modeling to incorporate faster time scales associated with mechanical relaxation [49,50], and to develop new efficient computational methods [28,51–53].

The PFC model can be connected to microscopic theory via classical density functional theory (DFT) of freezing [25,33,54–56]. It has been found that the PFC free energy functional can be derived from classical DFT for either pure materials or binary mixtures [57–62], by approximating the two-point direct correlation function with a truncated Fourier series and expanding the ideal-gas part of the DFT free energy functional in a power series of ρ and ψ (up to fourth order) [25]. While this connection provides insight into the parameters that enter PFC models, the approximations used are quite drastic and the resulting model is a poor approximation of classical DFT [56]. A similar connection could be made with the atomic density formulation of Jin and Khachaturyan [63] which is similar in form to the classical DFT, although the parameters that enter are given a different physical interpretation.

The main difficulty in directly simulating classical DFT is that the solutions for ρ are very sharply peaked around the lattice positions (at least in metallic crystals), while simple PFC models predict very smooth sinusoidal profiles. This difference makes numerical simulations of a simple PFC model much simpler than classical DFT as the former model's grid spacing can be a factor of ten larger than the latter's, so that in three dimensions a PFC model can simulate systems three orders of magnitudes larger than classical DFT with the same memory requirements. In addition it has been shown that a simple PFC can be adjusted to match many material properties, such as surface energy and its anisotropy, bulk moduli, and the miscibility gap in three-dimensional (3D) bcc iron [56] and the velocity of liquid/solid fronts in two-dimensional (2D) hexagonal crystal of colloids [33].

Another benefit of PFC modeling is the ability to efficiently simulate microstructure dynamics. At present, PFC dynamics has been largely introduced phenomenologically using time-dependent Ginzburg-Landau type dynamics [23,25]. Recent progress includes the derivation of hydrodynamic evolution equations for crystalline solids based on the Poisson bracket formalism and the simplification to PFC equations [54,55]. Very recently research has been conducted to connect the PFC-type models with microscopic dynamics (Smoluchowski equation) via dynamical density functional theory (DDFT) [33]. These results were also based on the truncation of DFT free energy up to two-point correlation function, and for single-component systems.

In this paper we provide a systematic derivation of PFC dynamics from DDFT, for both single-component and binary systems that involve the evolution of atomic number density and alloy concentration fields (see Sec. II). Our derivation includes contributions from three-point direct correlation functions, which have been shown important for the DFT calculations [64,65]. The original PFC models can be recovered via the lowest order approximation of our DDFT results, with the PFC parameters being connected to quantities of DFT correlation functions. Our calculations can be directly extended to incorporate fourth and higher-order correlation functions in DFT.

To complete the PFC methodology for binary systems, the full amplitude equation formalism is established for a 2D system with hexagonal/triangular crystalline symmetry. It incorporates the effects of species-dependent atomic mobility and average (zeroth-mode) atomic density that are usually coupled with the dynamics of structural amplitudes and concentration field during system evolution but absent in previous studies of binary PFC. As shown in Sec. III, the standard multiple-scale expansion is first applied to derive the lowest order amplitude equations, followed by a hybrid approach that we develop here to obtain the equations incorporating all orders of expansion. Furthermore, stochastic amplitude equations are derived for both single-component and binary PFC models, showing the corresponding noise dynamics as well as its coupling due to different atomic mobilities of system components (see Sec. IV).

As has been discussed in previous research, the advantage of the amplitude equation representation can be revealed via its large increase of computational efficiency due to the large length and time scales involved [26,27,30] and also its amenability to advanced numerical schemes such as adaptive mesh refinement method [28]. Furthermore, these amplitude equations are more amenable to analytic calculations as shown in recent studies of surface nanostructure formation in strained epitaxial films [3,37] as well as in most recent results for establishing the correspondence between PFC type models and traditional phase field approaches [32]. To further illustrate these advantages, in Sec. V we present a sample application of the derived binary PFC amplitude equations to the phenomenon of surface segregation and alloy intermixing. This is of particular importance in material growth (e.g., group VI or III-V semiconductor thin film epitaxy [66–73]), but rather limited information and understanding is available to date. We focus on both liquid-solid(crystal) coexistence profile and the coherent growth of strained solid layers, and show the control of intra- and interlayer diffusion by varying material parameters including solute expansion coefficient (due to different atomic sizes), misfit strain in alloy layers, and the mobility difference between alloy components. This study provides an understanding of mass transport mechanisms during material growth and evolution. The dynamic processes of strained layer growth as well as the associated composition overshooting phenomenon are obtained in our calculations in Sec. V. The results are compared to experimental findings of vertical composition segregation or surface enrichment as widely encountered during the growth of various alloy heterostructure systems such as InAs/GaAs, Ge/Si, GaAs/GaSb, InP/InGaAs, etc. [66–73].

II. DERIVATION OF PFC DYNAMICS VIA DYNAMICAL DENSITY FUNCTIONAL THEORY

A. Single-component systems

We start from the DDFT equation governing the evolution of a time-dependent local atomic number density field $\rho(\boldsymbol{r},t)$,

$$\frac{\partial\rho(\boldsymbol{r},t)}{\partial t} = \boldsymbol{\nabla}\cdot\left[M\rho(\boldsymbol{r},t)\,\boldsymbol{\nabla}\frac{\delta\mathcal{F}}{\delta\rho}\right], \tag{1}$$

which was first proposed phenomenologically [74,75] and was later derived by various groups via microscopic Brownian dynamics [76–78] and Hamiltonian dynamics and hydrodynamics [79] (see Ref. [33] for a brief review). The DDFT equations for binary A/B systems are similar to Eq. (1), with $\rho(\boldsymbol{r},t)$ replaced by $\rho_i(\boldsymbol{r},t)$ $(i=A,B$; see Sec. II B below), which has also been derived recently from Brownian dynamics (the Smoluchowski equation) [80]. In Eq. (1) the mobility is $M=D/k_BT$, where D is the diffusion coefficient and T is temperature.

In classical DFT the free energy functional $\mathcal{F}$ can be expanded as [57,58]

$$\begin{aligned}\frac{\mathcal{F}[\rho]}{k_BT} = &\int d\boldsymbol{r}[\rho\,\ln(\rho/\rho_l)-\delta\rho]\\ &-\frac{1}{2!}\int d\boldsymbol{r}_1d\boldsymbol{r}_2\delta\rho(\boldsymbol{r}_1)C^{(2)}(\boldsymbol{r}_1,\boldsymbol{r}_2)\delta\rho(\boldsymbol{r}_2)\\ &-\frac{1}{3!}\int d\boldsymbol{r}_1d\boldsymbol{r}_2d\boldsymbol{r}_3C^{(3)}(\boldsymbol{r}_1,\boldsymbol{r}_2,\boldsymbol{r}_3)\delta\rho(\boldsymbol{r}_1)\delta\rho(\boldsymbol{r}_2)\delta\rho(\boldsymbol{r}_3)\\ &+\cdots,\end{aligned} \tag{2}$$

where ρ_l is the reference liquid state density taken at liquid/solid coexistence, $\delta\rho=\rho-\rho_l$ and $C^{(n)}$ is the n-point direct correlation function of the liquid phase at ρ_l. It is important that the correlation functions are taken from the liquid state to maintain rotational invariance. Details of the correlation functions depend on the specific material systems studied and are usually calculated via various approximations [59,61,62]. Following the original PFC approach [25], the Fourier component of the two-point correlation function $\hat{C}^{(2)}$ is expanded as a power series of wavenumber q to fit up to its first peak, i.e.,

$$\hat{C}^{(2)}(q) = -\hat{C}_0+\hat{C}_2q^2-\hat{C}_4q^4+\cdots, \tag{3}$$

where $\hat{C}_0$, $\hat{C}_2$, and $\hat{C}_4$ are fitting parameters that can be connected to material properties such as isothermal compressibility of liquid phase, bulk modulus and lattice constant of crystal state [25,56]. For the three-point correlation function C_3, its Fourier transform yields

$$C^{(3)}(\boldsymbol{r}_1,\boldsymbol{r}_2,\boldsymbol{r}_3) = \frac{1}{(2\pi)^6}\int d\boldsymbol{q}d\boldsymbol{q}'e^{i\boldsymbol{q}\cdot(\boldsymbol{r}_1-\boldsymbol{r}_2)}e^{i\boldsymbol{q}\cdot(\boldsymbol{r}_2-\boldsymbol{r}_3)}\hat{C}^{(3)}(\boldsymbol{q},\boldsymbol{q}').$$

The simplest approximation is to keep only the zero wavenumber mode, i.e.,

$$\hat{C}^{(3)}(\boldsymbol{q},\boldsymbol{q}') \simeq \hat{C}^{(3)}(\boldsymbol{q}=\boldsymbol{q}'=0) = -\hat{C}_0^{(3)}, \tag{4}$$

as adopted in the DFT studies of hard spheres [64,81] and Lennard-Jones mixtures [82]. This can be justified from the previous results of hard-spheres DFT calculations that nonzero wavenumber components of $\hat{C}^{(3)}$ have been shown to yield minor contributions [64,81] and that as order n increases, the oscillation details of $\hat{C}^{(n)}$ become less and less relevant compared to the zero wavenumber mode [83].

Defining the rescaled atomic density field $n=(\rho-\rho_l)/\rho_l$ and using the approximations (3) and (4), the free energy functional (2) becomes

$$\begin{aligned}\Delta\mathcal{F}/\rho_lk_BT = \int d\boldsymbol{r}\Bigg[&(1+n)\ln(1+n)+\frac{1}{2}B^xn(2R^2\nabla^2+R^4\nabla^4)n\\ &+\frac{1}{2}B_l'n^2+\frac{1}{3}\tilde{B}n^3\Bigg],\end{aligned} \tag{5}$$

where $\Delta\mathcal{F}=\mathcal{F}[\rho]-\mathcal{F}[\rho_l]$, and

$$\begin{aligned}&B_l'=\rho_l\hat{C}_0=B^\ell-1,\quad B^x=\rho_l\hat{C}_2^2/4\hat{C}_4,\quad R=\sqrt{2\hat{C}_4/\hat{C}_2},\\ &\tilde{B}=\rho_l^2\hat{C}_0^{(3)}/2.\end{aligned} \tag{6}$$

Substituting Eq. (5) into the DDFT Eq. (1), which can be rewritten as

$$\frac{\partial n}{\partial t} = M'\,\boldsymbol{\nabla}\cdot\left[(1+n)\,\boldsymbol{\nabla}\frac{\delta\mathcal{F}}{\delta n}\right] \tag{7}$$

(with $M'=M/\rho_l$), we find [84]

$$\begin{aligned}\frac{\partial n}{\partial t} = &D\{\nabla^2[-(B^x-B^\ell)n+B^x(R^2\nabla^2+1)^2n+\tau n^2+vn^3]\\ &+B^x\,\boldsymbol{\nabla}\cdot[n\,\boldsymbol{\nabla}(R^2\nabla^2+1)^2n]\},\end{aligned} \tag{8}$$

where $\tau=-(B^x-B^\ell+1)/2+\tilde{B}$, $v=2\tilde{B}/3$, and we have used the relation $M=D/k_BT$. Note that if only the two-point correlation function in the DFT free energy (2) was used it would yield $\tilde{B}=v=0$, and Eq. (8) reduces to a form equivalent to the PFC1 model given in Ref. [33]. However, this would then be a second-order dynamic equation due to the absence of n^3 term, and as found in our numerical tests, is more difficult to converge at long enough time compared to the full third-order Eq. (8).

It is convenient to rescale Eq. (8) via a length scale R, a time scale R^2/DB^x, and $n\to\sqrt{v/B^x}n$, leading to

$$\begin{aligned}\frac{\partial n}{\partial t} = &\nabla^2[-\epsilon n+(\nabla^2+q_0^2)^2n+g_2n^2+n^3]+g_0\,\boldsymbol{\nabla}\\ &\cdot[n\,\boldsymbol{\nabla}(\nabla^2+q_0^2)^2n],\end{aligned} \tag{9}$$

where

$$\epsilon=(B^x-B^\ell)/B^x,\quad q_0=1,\quad g_2=\tau/\sqrt{vB^x},\quad g_0=\sqrt{B^x/v}. \tag{10}$$

The original PFC equation is recovered by considering that $(\boldsymbol{\nabla}\cdot[n\boldsymbol{\nabla}(\nabla^2+q_0^2)^2n])$ is of higher-order compared to term $\nabla^2(\nabla^2+q_0^2)^2n$. This can be obtained via a simple scale analy-

sis: $n \sim \mathcal{O}(\epsilon^{1/2})$ and $(\nabla^2+q_0^2)^2 n \sim \mathcal{O}(\epsilon^{3/2})$ (see also Sec. III A for more detail of scale expansion). Thus to lowest order approximation, Eq. (9) can be reduced to the original PFC model equation that has been widely used,

$$\frac{\partial n}{\partial t} = \nabla^2[-\epsilon n + (\nabla^2 + q_0^2)^2 n + g_2 n^2 + n^3]. \tag{11}$$

This derivation procedure can be readily extended to incorporate higher-order direct correlation functions of DFT (e.g., four-point, five-point, etc.) and thus to include higher-order terms such as n^4, $n^5, \ldots$, in the PFC model. Similarly, these high-order correlation functions can be effectively approximated to lowest order via the zero wavenumber modes, based on the recent DFT calculations [83]. For example, the contribution $\mathcal{F}^{(4)}$ of free energy functional from the four-point correlation function is given by

$$\mathcal{F}^{(4)}/k_B T = -\frac{1}{24}\int d\boldsymbol{r}_1 d\boldsymbol{r}_2 d\boldsymbol{r}_3 d\boldsymbol{r}_4 C^{(4)}(\boldsymbol{r}_1,\boldsymbol{r}_2,\boldsymbol{r}_3,\boldsymbol{r}_4) \times \delta\rho(\boldsymbol{r}_1)\delta\rho(\boldsymbol{r}_2)\delta\rho(\boldsymbol{r}_3)\delta\rho(\boldsymbol{r}_4). \tag{12}$$

Assuming $\hat{C}^{(4)}(\boldsymbol{q},\boldsymbol{q}',\boldsymbol{q}'') \simeq \hat{C}^{(4)}(\boldsymbol{q}=\boldsymbol{q}'=\boldsymbol{q}''=0) = -\hat{C}_0^{(4)}$, the free energy functional (5) is now

$$\Delta\mathcal{F}/\rho_l k_B T = \int d\boldsymbol{r}\left[(1+n)\ln(1+n) + \frac{1}{2}B^x n(2R^2\nabla^2 + R^4\nabla^4)n + \frac{1}{2}B_l' n^2 + \frac{1}{3}\tilde{B} n^3 + \frac{1}{4}\tilde{B}_4 n^4\right], \tag{13}$$

where $\tilde{B}_4 = \rho_l^3 \hat{C}_0^{(4)}/6$. The dynamic equation for n would then be

$$\frac{\partial n}{\partial t} = D\{\nabla^2[-(B^x - B^\ell)n + B^x(R^2\nabla^2+1)^2 n + \tau n^2 + v n^3 + u n^4] + B^x \nabla\cdot[n(R^2\nabla^2+1)^2 \nabla n]\}, \tag{14}$$

where $v = 2\tilde{B}/3 + \tilde{B}_4$ and $u = 3\tilde{B}_4/4$. Again the last term of Eq. (14) is of higher order and can be neglected in the lowest order approximation.

B. Binary systems

For a binary system with components A and B, the DDFT equations describing the dynamics of the respective atomic density fields ρ_A and ρ_B are given by [80]

$$\frac{\partial \rho_A}{\partial t} = \nabla\cdot\left[M_A\rho_A\nabla\frac{\delta\mathcal{F}}{\delta\rho_A}\right], \quad \frac{\partial \rho_B}{\partial t} = \nabla\cdot\left[M_B\rho_B\nabla\frac{\delta\mathcal{F}}{\delta\rho_B}\right], \tag{15}$$

where $M_{A(B)}$ is the atomic mobility for specie A (B). The corresponding classical density functional free energy (hereafter referred to as "DFT" for short) is of the form [59–62]

$$\mathcal{F}/k_B T = \int d\boldsymbol{r}\sum_{i=A,B}\left[\rho_i \ln\frac{\rho_i}{\rho_l^i} - \delta\rho_i\right] - \sum_{n=2}^{\infty}\frac{1}{n!}\int d\boldsymbol{r}_1\cdots d\boldsymbol{r}_n \times \sum_{i,\ldots,j=A,B} C_{i\ldots j}^{(n)}(\boldsymbol{r}_1,\cdots,\boldsymbol{r}_n)\delta\rho_i(\boldsymbol{r}_1)\cdots\delta\rho_j(\boldsymbol{r}_n), \tag{16}$$

where ρ_l^i is the reference liquid state density of component i, $\delta\rho_i = \rho_i - \rho_l^i$, and $C_{i\ldots j}^{(n)}$ refers to the n-point direct correlation function between components $i,\ldots,j=A,B$. Up to three-point correlation functions, we have

$$\begin{aligned}\mathcal{F}/k_B T = &\int d\boldsymbol{r}[\rho_A \ln(\rho_A/\rho_l^A) - \delta\rho_A + \rho_B\ln(\rho_B/\rho_l^B) - \delta\rho_B] \\ &-\frac{1}{2}\int d\boldsymbol{r}_1 d\boldsymbol{r}_2[\delta\rho_A(\boldsymbol{r}_1)C_{AA}^{(2)}(\boldsymbol{r}_1,\boldsymbol{r}_2)\delta\rho_A(\boldsymbol{r}_2) \\ &+\delta\rho_B(\boldsymbol{r}_1)C_{BB}^{(2)}(\boldsymbol{r}_1,\boldsymbol{r}_2)\delta\rho_B(\boldsymbol{r}_2) \\ &+2\delta\rho_A(\boldsymbol{r}_1)C_{AB}^{(2)}(\boldsymbol{r}_1,\boldsymbol{r}_2)\delta\rho_B(\boldsymbol{r}_2)] \\ &-\frac{1}{6}\int d\boldsymbol{r}_1 d\boldsymbol{r}_2 d\boldsymbol{r}_3[C_{AAA}^{(3)}(\boldsymbol{r}_1,\boldsymbol{r}_2,\boldsymbol{r}_3)\delta\rho_A(\boldsymbol{r}_1) \\ &\times\delta\rho_A(\boldsymbol{r}_2)\delta\rho_A(\boldsymbol{r}_3) \\ &+C_{BBB}^{(3)}(\boldsymbol{r}_1,\boldsymbol{r}_2,\boldsymbol{r}_3)\delta\rho_B(\boldsymbol{r}_1)\delta\rho_B(\boldsymbol{r}_2)\delta\rho_B(\boldsymbol{r}_3) \\ &+3C_{AAB}^{(3)}(\boldsymbol{r}_1,\boldsymbol{r}_2,\boldsymbol{r}_3)\delta\rho_A(\boldsymbol{r}_1)\delta\rho_A(\boldsymbol{r}_2)\delta\rho_B(\boldsymbol{r}_3) \\ &+3C_{ABB}^{(3)}(\boldsymbol{r}_1,\boldsymbol{r}_2,\boldsymbol{r}_3)\delta\rho_A(\boldsymbol{r}_1)\delta\rho_B(\boldsymbol{r}_2)\delta\rho_B(\boldsymbol{r}_3)].\end{aligned} \tag{17}$$

Similar to the single-component case discussed in Sec. II A, the correlation functions $C_{ij}^{(2)}(\boldsymbol{r}_1,\boldsymbol{r}_2)$ and $C_{ijk}^{(3)}(\boldsymbol{r}_1,\boldsymbol{r}_2,\boldsymbol{r}_3)$ $(i,j,k=A,B)$ are expanded in Fourier space as

$$\hat{C}_{ij}^{(2)}(q) = -\hat{C}_0^{ij} + \hat{C}_2^{ij}q^2 - \hat{C}_4^{ij}q^4 + \cdots,$$

$$\hat{C}_{ijk}^{(3)}(\boldsymbol{q},\boldsymbol{q}') \simeq \hat{C}_{ijk}^{(3)}(\boldsymbol{q}=\boldsymbol{q}'=0) = -\hat{C}_0^{ijk}. \tag{18}$$

As in the original binary PFC model, we introduce an atomic density field n and a concentration field ψ via

$$n = \frac{\rho-\rho_l}{\rho_l} = \frac{\rho_A+\rho_B-\rho_l}{\rho_l}, \quad \psi = \frac{\rho_A-\rho_B}{\rho} = \frac{\rho_A-\rho_B}{\rho_A+\rho_B}, \tag{19}$$

where $\rho_l = \rho_l^A + \rho_l^B$, and hence

$$\rho_A = \frac{\rho_l}{2}(1+n)(1+\psi), \quad \rho_B = \frac{\rho_l}{2}(1+n)(1-\psi). \tag{20}$$

Substituting Eqs. (18)–(20) into Eq. (17), we can express the free energy functional in terms of n and ψ,

$$\Delta\mathcal{F}/\rho_l k_B T = \int d\boldsymbol{r}\left\{(1+n)\ln(1+n) + \frac{1}{2}(1+n)[(1+\psi)\ln(1+\psi) + (1-\psi)\ln(1-\psi)] + \beta(\psi)n + \frac{1}{2}B_l'(\psi)n^2 + \frac{1}{3}\tilde{B}(\psi)n^3 + \frac{1}{2}\beta_2\psi^2 + \frac{1}{3}\beta_3\psi^3\right.$$

$$+\frac{(1+n)}{2}(2B^x(\psi)R^2\nabla^2+B^x(\psi)R^4\nabla^4)n$$
$$+\frac{K}{2}|\nabla[(1+n)\psi]|^2+\frac{\kappa}{2}(\nabla^2[(1+n)\psi])^2\Bigg\}, \quad (21)$$

where

$$\beta(\psi)=\beta_0\psi+\beta_1\psi^2+\beta_3\psi^3=\frac{\rho_l}{4}\left[\delta\hat{C}_0+\frac{\rho_l^B-\rho_l^A}{2}\delta\hat{C}_0^{(3)}\right]\psi$$
$$+\left[\beta_2+\frac{\rho_l^2}{16}\delta\hat{C}_0^{(3)}\right]\psi^2+\frac{\rho_l^2}{16}\Delta\hat{C}_0^{(3)}\psi^3,$$

$$B_l'(\psi)=B^\ell(\psi)-1=B_0^\ell-1+B_1^\ell\psi+B_2^\ell\psi^2+B_3^\ell\psi^3$$
$$=\rho_l\left[\hat{\bar{C}}_0+\frac{\rho_l^B-\rho_l^A}{8}\hat{\bar{C}}_0^{(3)}\right]+\frac{\rho_l}{2}\left[\delta\hat{C}_0+\frac{\rho_l^B-\rho_l^A}{2}\delta\hat{C}_0^{(3)}\right.$$
$$\left.+\frac{\rho_l}{4}\hat{\bar{C}}_0^{(3)}\right]\psi+\frac{\rho_l}{4}\left[\Delta\hat{C}_0+\frac{\rho_l^B-\rho_l^A}{2}\Delta\hat{C}_0^{(3)}+\rho_l\delta\hat{C}_0^{(3)}\right]\psi^2$$
$$+\frac{\rho_l^2}{8}\Delta\hat{C}_0^{(3)}\psi^3,$$

$$\tilde{B}(\psi)=\frac{\rho_l^2}{16}[8\hat{\bar{C}}_0^{(3)}+3\hat{\tilde{C}}_0^{(3)}\psi+3\delta\hat{C}_0^{(3)}\psi^2+\Delta\hat{C}_0^{(3)}\psi^3]$$
$$=\tilde{B}_0+\tilde{B}_1\psi+\tilde{B}_2\psi^2+\beta_3\psi^3,$$

$$\beta_2=\frac{\rho_l}{4}\left[\Delta\hat{C}_0+\frac{\rho_l^B-\rho_l^A}{2}\Delta\hat{C}_0^{(3)}\right],$$

$$\Delta\beta=\beta_1-\beta_2=\frac{\rho_l^2}{16}\delta\hat{C}_0^{(3)}, \quad \tilde{B}_2=3\Delta\beta,$$

$$B_1^\ell=2\beta_0+\frac{2}{3}\tilde{B}_1, \quad B_2^\ell=4\beta_1-3\beta_2, \quad B_3^\ell=2\beta_3,$$

$$B^x(\psi)=\frac{\rho_l(\hat{\bar{C}}_2+\delta\hat{C}_2\psi/2)^2}{4(\hat{\bar{C}}_4+\delta\hat{C}_4\psi/2)}$$
$$=\frac{\rho_l\hat{\bar{C}}_2^2}{4\hat{\bar{C}}_4}\left[1+\left(\frac{\delta\hat{C}_2}{\hat{\bar{C}}_2}-\frac{\delta\hat{C}_4}{2\hat{\bar{C}}_4}\right)\psi+\cdots\right]$$
$$=B_0^x+B_1^x\psi+\cdots,$$

$$R=\sqrt{\frac{2(\hat{\bar{C}}_4+\delta\hat{C}_4\psi/2)}{\hat{\bar{C}}_2+\delta\hat{C}_2\psi/2}}$$
$$=\sqrt{\frac{2\hat{\bar{C}}_4}{\hat{\bar{C}}_2}}\left[1+\frac{1}{4}\left(\frac{\delta\hat{C}_4}{\hat{\bar{C}}_4}-\frac{\delta\hat{C}_2}{\hat{\bar{C}}_2}\right)\psi+\cdots\right]$$
$$=R_0+R_1\psi+\cdots,$$

$$B^xR^2=\frac{\rho_l}{2}\left(\hat{\bar{C}}_2+\frac{1}{2}\delta\hat{C}_2\psi\right)=B_0^xR_0^2(1+\alpha_2\psi), \quad \alpha_2=\delta\hat{C}_2/2\hat{\bar{C}}_2,$$

$$B^xR^4=\rho_l\left(\hat{\bar{C}}_4+\frac{1}{2}\delta\hat{C}_4\psi\right)=B_0^xR_0^4(1+\alpha_4\psi), \quad \alpha_4=\delta\hat{C}_4/2\hat{\bar{C}}_4,$$

$$K=-\frac{\rho_l}{4}\Delta\hat{C}_2, \quad \kappa=\frac{\rho_l}{4}\Delta\hat{C}_4. \quad (22)$$

In the above formulas, the following has been defined from the correlation functions:

$$\bar{C}=\frac{1}{4}(C_{AA}^{(2)}+C_{BB}^{(2)}+2C_{AB}^{(2)}),$$

$$\delta C=C_{AA}^{(2)}-C_{BB}^{(2)},$$

$$\Delta C=C_{AA}^{(2)}+C_{BB}^{(2)}-2C_{AB}^{(2)},$$

$$\bar{C}^{(3)}=\frac{1}{8}(C_{AAA}^{(3)}+C_{BBB}^{(3)}+3C_{AAB}^{(3)}+3C_{ABB}^{(3)}),$$

$$\tilde{C}^{(3)}=C_{AAA}^{(3)}-C_{BBB}^{(3)}+C_{AAB}^{(3)}-C_{ABB}^{(3)},$$

$$\delta C^{(3)}=C_{AAA}^{(3)}+C_{BBB}^{(3)}-C_{AAB}^{(3)}-C_{ABB}^{(3)}, \quad (23)$$

$$\Delta C^{(3)}=C_{AAA}^{(3)}-C_{BBB}^{(3)}-3C_{AAB}^{(3)}+3C_{ABB}^{(3)},$$

and the "ˆ" in Eq. (22) refer to the Fourier coefficients in the expansions of Eq. (18) where the numerical subscripts on the coefficients refer to the appropriate power of the expansion. For binary alloys the lattice constant is often approximated by Vegard's law, i.e., $R \simeq R_0+R_1\psi=R_0(1+\alpha\psi)$. In this expansion, near $\psi=0$ the solute expansion coefficient α is expressed as

$$\alpha=R_1/R_0=\frac{1}{2}(\alpha_4-\alpha_2). \quad (24)$$

(In the dilute limit (i.e., $\psi\sim\pm1$) it would be simple to expand R around $\psi\sim\pm1$ to obtain the solute expansion coefficient as well.) Using the simplification adopted in the original binary PFC [32], it is assumed that $B^x \simeq B_0^x$ and $R^2 \simeq R_0^2(1+2\alpha\psi)$, $R^4 \simeq R_0^4(1+4\alpha\psi)$ via expansion, which corresponds to the assumption of $\alpha_2 \simeq 2\alpha$ and $\alpha_4 \simeq 4\alpha$ as obtained from Eqs. (22) and (24).

In terms of the above definitions, the time derivatives of the variables n and ψ defined in Eq. (19) are given by

$$\frac{\partial n}{\partial t}=\frac{1}{\rho_l}\left(\frac{\partial\rho_A}{\partial t}+\frac{\partial\rho_B}{\partial t}\right),$$

$$\frac{\partial\psi}{\partial t}=\frac{1}{\rho_l(1+n)}\left[(1-\psi)\frac{\partial\rho_A}{\partial t}-(1+\psi)\frac{\partial\rho_B}{\partial t}\right]. \quad (25)$$

From the DDFT Eqs. (15), the dynamics for n and ψ thus become

$$\partial n/\partial t = M_1\mathcal{D}_1 + M_2\mathcal{D}_2,$$

$$\partial \psi/\partial t = \frac{1}{1+n}[(M_2 - M_1\psi)\mathcal{D}_1 + (M_1 - M_2\psi)\mathcal{D}_2], \quad (26)$$

where

$$M_1 = \frac{1}{2}k_BT(M_A + M_B), \quad M_2 = \frac{1}{2}k_BT(M_A - M_B), \quad (27)$$

and

$$\mathcal{D}_1 = \frac{1}{\rho_l k_B T}\left\{\boldsymbol{\nabla}\cdot\left[(1+n)\,\boldsymbol{\nabla}\frac{\delta\mathcal{F}}{\delta n}\right] - \boldsymbol{\nabla}\cdot\left[(\boldsymbol{\nabla}\psi)\frac{\delta\mathcal{F}}{\delta\psi}\right]\right\},$$

$$\mathcal{D}_2 = \frac{1}{\rho_l k_B T}\left\{\boldsymbol{\nabla}\cdot\left[(1+n)\psi\,\boldsymbol{\nabla}\frac{\delta\mathcal{F}}{\delta n}\right] + \boldsymbol{\nabla}\cdot\left[(1+n)(1-\psi^2)\,\boldsymbol{\nabla}\left(\frac{1}{1+n}\frac{\delta\mathcal{F}}{\delta\psi}\right) - (\psi\boldsymbol{\nabla}\psi)\frac{\delta\mathcal{F}}{\delta\psi}\right]\right\}. \quad (28)$$

Using the free energy functional (21) as well as Eq. (28), the results of $\mathcal{D}_1$ and $\mathcal{D}_2$ (keeping all the terms) are

$$\begin{aligned}\mathcal{D}_1 = \nabla^2\Bigg\{&-(B_0^x - B_0^\ell)n + (B_1^\ell\psi + B_2^\ell\psi^2)n + [-(B_0^x - B_0^\ell + 1)/2 + \tilde{B}_0 + (B_1^\ell/2 + \tilde{B}_1)\psi + (B_2^\ell/2 + \tilde{B}_2)\psi^2]n^2 \\ &+ \frac{2}{3}(\tilde{B}_0 + \tilde{B}_1\psi + \tilde{B}_2\psi^2)n^3 + \frac{1}{3}B_3^\ell(1+n)^3\psi^3 + \beta_0\psi + \frac{1}{2}(\beta_1 + \Delta\beta)\psi^2 + B_0^x(R_0^2\nabla^2 + 1)^2 n + B_0^x\left(\alpha_2 R_0^2\nabla^2 + \frac{\alpha_4}{2}R_0^4\nabla^4\right)[(1+n)\psi]\Bigg\} \\ &+ \boldsymbol{\nabla}\cdot\left\{n\,\boldsymbol{\nabla}\left[B_0^x(R_0^2\nabla^2 + 1)^2 n + B_0^x\left(\alpha_2 R_0^2\nabla^2 + \frac{\alpha_4}{2}R_0^4\nabla^4\right)[(1+n)\psi]\right]\right\} + \boldsymbol{\nabla}\cdot\left\{(1+n)\psi\,\boldsymbol{\nabla}\left[B_0^x\left(\alpha_2 R_0^2\nabla^2 + \frac{\alpha_4}{2}R_0^4\nabla^4\right)n\right.\right. \\ &\left.\left. + (-K\nabla^2 + \kappa\nabla^4)[(1+n)\psi]\right]\right\}, \end{aligned} \quad (29)$$

$$\begin{aligned}\mathcal{D}_2 = \nabla^2\Bigg\{&\beta_0 n + (\beta_0/2 + \tilde{B}_1/3)n^2 + \frac{2}{9}\tilde{B}_1 n^3 + (1 + \beta_2 + 2\Delta\beta n)(1+n)\psi + \frac{1}{2}(\beta_0 + B_3^\ell)(1+n)^2\psi^2 + \frac{1}{3}\tilde{B}_1 n^2\psi^2 \\ &+ \frac{2}{3}\Delta\beta(1+n)^3\psi^3 + B_0^x\left(\alpha_2 R_0^2\nabla^2 + \frac{\alpha_4}{2}R_0^4\nabla^4\right)n + (-K\nabla^2 + \kappa\nabla^4)[(1+n)\psi]\Bigg\} \\ &+ \boldsymbol{\nabla}\cdot\left\{n\,\boldsymbol{\nabla}\left[(1+n)(\beta_2 + 2\Delta\beta n)\psi + \beta_3(1+n)^2\psi^2 + B_0^x\left(\alpha_2 R_0^2\nabla^2 + \frac{\alpha_4}{2}R_0^4\nabla^4\right)n + (-K\nabla^2 + \kappa\nabla^4)[(1+n)\psi]\right]\right\} \\ &+ \boldsymbol{\nabla}\cdot\left\{\psi\,\boldsymbol{\nabla}\left[\frac{2}{3}\tilde{B}_1 n\psi\right]\right\} + \boldsymbol{\nabla}\cdot\left\{(1+n)\psi\,\boldsymbol{\nabla}\left[-(B_0^x - B_0^\ell + 1)n + \left(\tilde{B}_0 + \frac{2}{3}\tilde{B}_1\psi\right)n^2 + B_0^x(R_0^2\nabla^2 + 1)^2 n\right.\right. \\ &\left.\left. + B_0^x\left(\alpha_2 R_0^2\nabla^2 + \frac{\alpha_4}{2}R_0^4\nabla^4\right)[(1+n)\psi]\right]\right\}. \end{aligned} \quad (30)$$

At this point in the derivation it should be noted that no additional approximations beyond those going into the expansions of Eq. (18) have been introduced.

1. Nondimensional form of model

To simplify the results, the above binary PFC equations can be rescaled via defining a length scale R_0, a time scale $R_0^2/M_1B_0^x$, $n \to \sqrt{v/B_0^x}n$, and $\psi \to \sqrt{v/B_0^x}\psi$, yielding

$$\partial n/\partial t = \mathcal{D}_1 + m\mathcal{D}_2, \quad (31)$$

$$\partial \psi/\partial t = \frac{1}{1+g_0 n}[(m - g_0\psi)\mathcal{D}_1 + (1 - mg_0\psi)\mathcal{D}_2],$$

where

$$m = \frac{M_2}{M_1} = \frac{M_A - M_B}{M_A + M_B}, \quad g_0 = \sqrt{\frac{B_0^x}{v}}, \quad v = \frac{2}{3}\tilde{B}_0 = \frac{\rho_l^2}{3}\hat{\tilde{C}}_0^{(3)}. \quad (32)$$

If keeping only terms up to 3rd order quantities of n and ψ, the results of $\mathcal{D}_1$ and $\mathcal{D}_2$ are rescaled as

$$\mathcal{D}_1 = \nabla^2\Bigg\{-\epsilon n + (\nabla^2+q_0^2)^2 n + (g_1\psi + g\psi^2)n + (g_2+\bar{g}_2\psi)n^2 + n^3 + \bar{g}\psi + v_1\psi^2 + u_1\psi^3$$
$$+\left(\alpha_2\nabla^2 + \frac{\alpha_4}{2}\nabla^4\right)[(1+g_0 n)\psi]$$
$$+ g_0\psi\left(\alpha_2\nabla^2 + \frac{\alpha_4}{2}\nabla^4\right)n\Bigg\} + g_0\boldsymbol{\nabla}\cdot\left\{n\boldsymbol{\nabla}\left[(\nabla^2+q_0^2)^2 n + \left(\alpha_2\nabla^2 + \frac{\alpha_4}{2}\nabla^4\right)((1+g_0 n)\psi)\right]\right\}$$
$$+ g_0\boldsymbol{\nabla}\cdot[\psi\boldsymbol{\nabla}(-K_0\nabla^2 + \kappa_0\nabla^4)$$
$$\times((1+g_0 n)\psi)] - g_0\boldsymbol{\nabla}\cdot\left[(\boldsymbol{\nabla}\psi)\left(\alpha_2\nabla^2 + \frac{\alpha_4}{2}\nabla^4\right)n\right]$$
$$+ g_0^2\boldsymbol{\nabla}\cdot\left\{n\psi\boldsymbol{\nabla}\left[\left(\alpha_2\nabla^2 + \frac{\alpha_4}{2}\nabla^4\right)n + (-K_0\nabla^2 + \kappa_0\nabla^4)\psi\right]\right\}, \tag{33}$$

$$\mathcal{D}_2 = \nabla^2\Bigg\{\bar{g}n + (1+g_0 n)\left(\alpha_2\nabla^2 + \frac{\alpha_4}{2}\nabla^4\right)n + (2v_1\psi + w_2\psi^2)n + (v_2 + g\psi)n^2 + g_3 n^3 + w_0\psi + v_0\psi^2 + u_0\psi^3$$
$$+ (-K_0\nabla^2 + \kappa_0\nabla^4)[(1+g_0 n)\psi]\Bigg\} + g_0\boldsymbol{\nabla}\cdot\{n\boldsymbol{\nabla}[w_0\psi + (-K_0\nabla^2 + \kappa_0\nabla^4)((1+g_0 n)\psi)]\}$$
$$- g_0\boldsymbol{\nabla}\cdot\left[(\boldsymbol{\nabla}n)\left(\alpha_2\nabla^2 + \frac{\alpha_4}{2}\nabla^4\right)n\right] + g_0\boldsymbol{\nabla}\cdot\left\{\psi\boldsymbol{\nabla}\left[(-\epsilon + \gamma_1\psi)n + \gamma_2 n^2 + (\nabla^2+q_0^2)^2 n + \left(\alpha_2\nabla^2 + \frac{\alpha_4}{2}\nabla^4\right)((1+g_0 n)\psi)\right]\right\}$$
$$+ g_0^2\boldsymbol{\nabla}\cdot\left\{n\psi\boldsymbol{\nabla}\left[(\nabla^2+q_0^2)^2 n + \left(\alpha_2\nabla^2 + \frac{\alpha_4}{2}\nabla^4\right)\psi\right]\right\}, \tag{34}$$

where the rescaled parameters are

$$\epsilon = \frac{B_0^x - B_0^\ell}{B_0^x}, \quad q_0 = 1, \quad g = \frac{B_2^\ell}{v},$$

$$g_2 = \frac{g_0}{2}\left(\frac{2\tilde{B}_0 - 1}{B_0^x} - \epsilon\right),$$

$$v_1 = \left(\frac{\beta_1 + \Delta\beta}{2B_0^x}\right)g_0,$$

$$w_0 = \frac{1+\beta_2}{B_0^x}, \quad u_0 = \frac{2\tilde{B}_2}{9v}, \quad K_0 = \frac{K}{B_0^x R_0^2} = -\frac{\Delta\hat{C}_2}{2\hat{\tilde{C}}_2},$$

$$\kappa_0 = \frac{\kappa}{B_0^x R_0^4} = \frac{\Delta\hat{C}_4}{4\hat{\tilde{C}}_4},$$

$$\bar{g} = \frac{\beta_0}{B_0^x}, \quad g_1 = \frac{B_1^\ell}{B_0^x}g_0, \quad \bar{g}_2 = \frac{B_1^\ell + 2\tilde{B}_1}{2v}, \quad u_1 = \frac{B_3^\ell}{3v},$$

$$w_2 = \frac{\beta_0 + 2B_3^\ell}{v}, \quad v_2 = \left(\frac{\beta_0/2 + \tilde{B}_1/3}{B_0^x}\right)g_0, \quad g_3 = \frac{2\tilde{B}_1}{9v},$$

$$v_0 = \left(\frac{\beta_0 + B_3^\ell}{2B_0^x}\right)g_0, \quad \gamma_1 = 3(g_3 - u_1)/g_0, \quad \gamma_2 = g_2 - v_1. \tag{35}$$

Note that from Eqs. (22) and (18), B_0^x can be rewritten as

$$B_0^x = \frac{\rho_l\hat{\tilde{C}}_2^2}{4\hat{\tilde{C}}_4} = \rho_l(\hat{\tilde{C}}_0 + \hat{\tilde{C}}_{\max}), \tag{36}$$

where $\hat{\tilde{C}}_{\max}$ is the maximum of the first peak of the two-point correlation function $\hat{\tilde{C}}$ in Fourier space. If $|\Delta\rho_l| = |\rho_l^A - \rho_l^B| \ll |\hat{\tilde{C}}_0/\hat{\tilde{C}}_0^{(3)}|$, $B_0^\ell \sim 1 + \rho_l\hat{\tilde{C}}_0$ from Eq. (22) and thus

$$\epsilon = \frac{B_0^x - B_0^\ell}{B_0^x} \sim \frac{\rho_l\hat{\tilde{C}}_{\max} - 1}{\rho_l(\hat{\tilde{C}}_0 + \hat{\tilde{C}}_{\max})} \sim \frac{\hat{\tilde{C}}_{\max}}{\hat{\tilde{C}}_0 + \hat{\tilde{C}}_{\max}}. \tag{37}$$

Usually $\hat{\tilde{C}}_{\max} \ll \hat{\tilde{C}}_0$ particularly when close to the melting point T_m, and hence ϵ can be viewed as a small variable (also used in amplitude equation expansion given below), proportional to $(T - T_m)/T_m$ as discussed in the original PFC model [25].

2. Simplification of scaled binary model

The rescaled PFC dynamic Eqs. (31)–(34) can be further simplified to a lower order form via a scale analysis. A

simple scale analysis of Eqs. (33) and (34) yields $n, \psi \sim \mathcal{O}(\epsilon^{1/2})$ [e.g., from Eq. (33) we have $\mathcal{O}(\epsilon n) \sim \mathcal{O}(n^3)$ and $\mathcal{O}(\psi) \sim \mathcal{O}(n)$, as is usually assumed]. To simplify the results the following approximations are made: (i) Assume that $\{|\hat{\bar{C}}_0|, |\hat{\bar{C}}_0^{(3)}|, |\delta\hat{C}_0^{(3)}|\} \gg \{|\delta\hat{C}_0|, |\hat{\bar{C}}_0^{(3)}|, |\Delta\hat{C}_0^{(3)}|\}$ and $|\rho_l^A - \rho_l^B| \ll |\rho_l^A + \rho_l^B|$. [An example case would be that the zeroth-mode ($q=0$) correlation functions between the same atomic species are of the same order, and are either significantly larger or significantly smaller than those between different ones; see Eq. (23).] Thus for the rescaled parameters in Eq. (35), we can estimate [based on the definitions in Eqs. (22) and (23), as well as Eqs. (32) and (36)] that

$$g_0, g, g_2, v_1, u_0 \sim \mathcal{O}(1) \text{ or } \mathcal{O}(\epsilon^{1/2}),$$

$$\bar{g}, g_1, \bar{g}_2, u_1, w_2, v_2, g_3, v_0, \gamma_1, \gamma_2 \sim \mathcal{O}(\epsilon) \text{ or higher}.$$

(ii) The concentration field ψ is slowly varying in space, and we can keep only the lowest linear gradient terms for ψ. (iii) Similar to the single-component case in Sec. II A, it can be argued that in Eqs. (33) and (34), compared to the first terms $\nabla^2\{\cdots\}$, all other terms ($g_0\nabla\cdot\{\cdots\}$) are of higher order. (iv) For linear terms in n, only $[-\varepsilon + (\nabla^2 + q_0^2)^2]n$ is kept which will lead to periodic crystal structure in solid phases, while the other term $(\alpha_2\nabla^2 + \frac{\alpha_4}{2}\nabla^4)n$ is neglected, which corresponds to ignoring the $n\psi$ related terms in the free energy functional (21) owing to the much larger length scales of ψ field [25]. (v) It is assumed that $\alpha_2 \simeq \alpha_4/2 \simeq 2\alpha$ [see the discussions below Eq. (24)].

To lowest order in $\mathcal{O}(\epsilon^{3/2})$ the above simplifications reduce the PFC Eqs. (31), (33), and (34) to

$$\partial n/\partial t = \mathcal{D}_1 + m\mathcal{D}_2, \quad \partial\psi/\partial t = m\mathcal{D}_1 + \mathcal{D}_2, \tag{38}$$

where

$$\mathcal{D}_1 = \nabla^2\{(-\epsilon + g\psi^2)n + (\nabla^2 + q_0^2)^2 n + g_2 n^2 + n^3 + v_1\psi^2 + 2\alpha_0[\psi(\nabla^2 + \nabla^4)n + (\nabla^2 + \nabla^4)(n\psi)]\},$$

$$\mathcal{D}_2 = \nabla^2[2\alpha_0 n(\nabla^2 + \nabla^4)n + (w_0 + 2v_1 n + gn^2)\psi + u_0\psi^3 - K_0\nabla^2\psi], \tag{39}$$

with $\alpha_0 = g_0\alpha$ the rescaled solute expansion coefficient. Equations (38) and (39) recover the original binary PFC model with conserved dynamics for both n and ψ fields [25,32], except for the v_1 terms ($v_1\psi^2$ and $2v_1 n\psi$), which account for additional coupling between the atomic density and concentration fields (or between small crystalline and "slow" concentration scales). This can also be seen via rewriting Eq. (39) through an effective potential (or free energy functional) $\mathcal{F}_{\text{eff}}$,

$$\mathcal{D}_1 = \nabla^2\frac{\delta\mathcal{F}_{\text{eff}}}{\delta n}, \quad \mathcal{D}_2 = \nabla^2\frac{\delta\mathcal{F}_{\text{eff}}}{\delta\psi}, \tag{40}$$

$$\mathcal{F}_{\text{eff}} = \int d\boldsymbol{r}\Big\{-\frac{1}{2}\epsilon n^2 + \frac{1}{2}n(\nabla^2 + q_0^2)^2 n + \frac{1}{3}g_2 n^3 + \frac{1}{4}n^4 + 2\alpha_0 n(\nabla^2 + \nabla^4)(n\psi) + \frac{1}{2}(w_0 + 2v_1 n + gn^2)\psi^2 + \frac{1}{4}u_0\psi^4 + \frac{1}{2}K_0|\nabla\psi|^2\Big\}. \tag{41}$$

In the rest of this work, all results, including the corresponding amplitude equation formalism, noise dynamics, and the related applications, are based on the simplified PFC dynamic Eqs. (38) and (39).

The above results can also be derived and verified through two other alternative methods, as given in Appendix A. Furthermore, to include higher-order terms (e.g., $n^4, \psi^4, \ldots$) in both the free energy functional and the dynamic equations, we need to consider higher-order direct correlation functions (four-point, five-point, etc.) as shown in the single-component case (Sec. II A), with similar derivation steps.

III. AMPLITUDE EQUATION FORMALISM FOR BINARY PFC MODEL

As discussed in Sec. I, the PFC methodology includes model equations governing the dynamics of density and concentration fields as given above. This section will examine the long wavelength and time limits of the alloy PFC model by deriving its corresponding amplitude equations, which emerge after coarse-graining the model using a multiple-scale analysis. The amplitude representation for single-component PFC models has been well established [26–30], while for binary systems the corresponding amplitude equations have been derived very recently, for both 2D hexagonal/triangular and 3D bcc and fcc crystalline structures [32,43]. Here we focus on the 2D amplitude equations for the binary PFC model with hexagonal lattice structure, yielding a complete formulation incorporating the effects of different mobilities between alloy components and dynamic variation of the average atomic density, both of which are missing in the previous binary alloy amplitude formulation [32]. It is straightforward to extend this calculation to 3D bcc or fcc structures. The derivation process involves two steps: the standard multiple-scale expansion [85] for lowest order amplitude equations (Sec. III A), and a new hybrid approach (combining results of multiple-scale approach and the idea of "Quick and Dirty" renormalization-group (RG) method developed by Goldenfeld *et al.* [26,27]) for full order amplitude equations (see Sec. III B). To apply the multiple-scale analysis, the rescaled PFC Eqs. (38) and (39) are used.

A. Multiple-scale expansion: Lowest order amplitude equations

Following the standard procedure of multiple-scale approach [85], in the limit of small ϵ (i.e., high temperature) we can separate "slow" spatial and temporal scales ($X = \epsilon^{1/2}x$, $Y = \epsilon^{1/2}y$, $T = \epsilon t$) for structural profile/amplitudes from "fast" scales of the underlying crystalline lattice. Substituting

$$\partial_x \to \partial_x + \epsilon^{1/2}\partial_X, \quad \partial_y \to \partial_y + \epsilon^{1/2}\partial_Y, \quad \partial_t \to \epsilon\partial_T, \quad (42)$$

and the expansions

$$n = \epsilon^{1/2}n^{(1/2)} + \epsilon n^{(1)} + \epsilon^{3/2}n^{(3/2)} + \epsilon^2 n^{(2)} + \cdots,$$

$$\psi = \epsilon^{1/2}\psi^{(1/2)} + \epsilon\psi^{(1)} + \epsilon^{3/2}\psi^{(3/2)} + \epsilon^2\psi^{(2)} + \cdots, \quad (43)$$

into the PFC Eqs. (38) and (39), we can obtain the corresponding equations at each order of $\epsilon^{1/2}$. For simplicity, assume $m, \alpha_0, g, u_0, K_0 \sim \mathcal{O}(1)$, $g_2, v_1 \sim \mathcal{O}(\epsilon^{1/2})$, and $w_0 \sim \mathcal{O}(\epsilon)$ (as also assumed in Sec. II B 2 for model simplification). To $\mathcal{O}(\epsilon^{1/2})$ and $\mathcal{O}(\epsilon)$ we have

$$\nabla^2[\mathcal{L}_0 n^{(i)} - mK_0\nabla^2\psi^{(i)}] = 0, \quad \nabla^2[m\mathcal{L}_0 n^{(i)} - K_0\nabla^2\psi^{(i)}] = 0, \quad (44)$$

where $i=1/2$ or 1, and $\mathcal{L}_0=(\nabla^2+q_0^2)^2$. This leads to $(1-m^2)\nabla^2\mathcal{L}_0 n^{(i)}=0$ and $(1-m^2)\nabla^4\psi^{(i)}=0$, with solutions

$$n^{(i)} = n_0^{(i)}(X,Y,T) + \sum_{j=1}^{3} A_j^{(i)}(X,Y,T)e^{i\boldsymbol{q}_j^0\cdot\boldsymbol{r}} + \text{c.c.},$$

$$\psi^{(i)} = \psi_0^{(i)}(X,Y,T), \quad (45)$$

where $\boldsymbol{q}_j^0$ represent the three reciprocal lattice vectors for 2D hexagonal/triangular structure: $\boldsymbol{q}_1^0=-q_0(\sqrt{3}\hat{x}/2+\hat{y}/2)$, $\boldsymbol{q}_2^0=q_0\hat{y}$, $\boldsymbol{q}_3^0=q_0(\sqrt{3}\hat{x}/2-\hat{y}/2)$. A_j are the slowly varying complex amplitudes of the modes $\boldsymbol{q}_j^0$, while n_0 and ψ_0 refer to the real amplitudes of the zero wavenumber neutral mode as a result of order parameter conservation [86].

Expanding to $\mathcal{O}(\epsilon^{3/2})$ yields (with $\boldsymbol{\nabla}_s=(\partial_X,\partial_Y)$, $\boldsymbol{\nabla}\cdot\boldsymbol{\nabla}_s=\partial_X\partial_X+\partial_Y\partial_Y$, and $\nabla_s^2=\partial_X^2+\partial_Y^2$)

$$\begin{aligned}
&\nabla^2\mathcal{L}_0 n^{(3/2)} - mK_0\nabla^4\psi^{(3/2)} \\
&\quad = \partial_T n^{(1/2)} + [\boldsymbol{\nabla}^2 - \boldsymbol{\nabla}^2(2\,\boldsymbol{\nabla}\cdot\boldsymbol{\nabla}_s)^2 - q_0^4\nabla_s^2]n^{(1/2)} \\
&\qquad - \nabla^2[g_2 n^{(1/2)^2} + n^{(1/2)^3}] - g\psi^{(1/2)^2}\nabla^2 n^{(1/2)} \\
&\qquad + 2\alpha_0\nabla^2[\psi^{(1/2)}(2\,\boldsymbol{\nabla}\cdot\boldsymbol{\nabla}_s)n^{(1/2)} \\
&\qquad + (2\,\boldsymbol{\nabla}\cdot\boldsymbol{\nabla}_s)(\psi^{(1/2)}n^{(1/2)})] \\
&\qquad + m\{2\alpha_0\nabla^2[n^{(1/2)}(2\,\boldsymbol{\nabla}\cdot\boldsymbol{\nabla}_s)n^{(1/2)}] \\
&\qquad - g\psi^{(1/2)}\nabla^2 n^{(1/2)^2} - 2v_1\psi^{(1/2)}\boldsymbol{\nabla}^2 n^{(1/2)}\},
\end{aligned}$$

$$\begin{aligned}
&m\nabla^2\mathcal{L}_0 n^{(3/2)} - K_0\nabla^4\psi^{(3/2)} \\
&\quad = m\{[\nabla^2 - \nabla^2(2\,\boldsymbol{\nabla}\cdot\boldsymbol{\nabla}_s)^2 - q_0^4\nabla_s^2]n^{(1/2)} - \nabla^2[g_2 n^{(1/2)^2} \\
&\qquad + n^{(1/2)^3}] - g\psi^{(1/2)^2}\nabla^2 n^{(1/2)} + 2\alpha_0\nabla^2[\psi^{(1/2)}(2\,\boldsymbol{\nabla}\cdot\boldsymbol{\nabla}_s)n^{(1/2)} \\
&\qquad + (2\,\boldsymbol{\nabla}\cdot\boldsymbol{\nabla}_s)(\psi^{(1/2)}n^{(1/2)})]\} + \partial_T\psi^{(1/2)} + 2\alpha_0\nabla^2[n^{(1/2)} \\
&\qquad \times(2\,\boldsymbol{\nabla}\cdot\boldsymbol{\nabla}_s)n^{(1/2)}] - g\psi^{(1/2)}\nabla^2 n^{(1/2)^2} - 2v_1\psi^{(1/2)}\nabla^2 n^{(1/2)},
\end{aligned}$$

which is equivalent to

$$\begin{aligned}
&(1-m^2)\nabla^2\mathcal{L}_0 n^{(3/2)} \\
&\quad = \partial_T n^{(1/2)} - m\partial_T\psi^{(1/2)} + (1-m^2)\{[\nabla^2 - \nabla^2(2\,\boldsymbol{\nabla}\cdot\boldsymbol{\nabla}_s)^2 \\
&\qquad - q_0^4\nabla_s^2]n^{(1/2)} - g\psi^{(1/2)^2}\nabla^2 n^{(1/2)} - \nabla^2[g_2 n^{(1/2)^2} + n^{(1/2)^3}] \\
&\qquad + 2\alpha_0\nabla^2[\psi^{(1/2)}(2\,\boldsymbol{\nabla}\cdot\boldsymbol{\nabla}_s)n^{(1/2)} \\
&\qquad + (2\,\boldsymbol{\nabla}\cdot\boldsymbol{\nabla}_s)(\psi^{(1/2)}n^{(1/2)})]\},
\end{aligned}$$

$$\begin{aligned}
&(1-m^2)K_0\nabla^4\psi^{(3/2)} \\
&\quad = m\partial_T n^{(1/2)} - \partial_T\psi^{(1/2)} + (1-m^2)\{-2\alpha_0\nabla^2 \\
&\qquad \times[n^{(1/2)}(2\,\boldsymbol{\nabla}\cdot\boldsymbol{\nabla}_s)n^{(1/2)}] + g\psi^{(1/2)}\nabla^2 n^{(1/2)^2} \\
&\qquad + 2v_1\psi^{(1/2)}\nabla^2 n^{(1/2)}\}. \quad (46)
\end{aligned}$$

As shown in Eq. (45), the zero eigenvectors of operators $\nabla^2\mathcal{L}_0$ and ∇^4 are $(e^{\pm i\boldsymbol{q}_j^0\cdot\boldsymbol{r}},1)$ and 1 (of the 0th mode), respectively. Using the Fredholm theorem or solvability condition [85] in Eq. (46), we can derive the lowest order amplitude equations as (with $j=1,2,3$)

$$\begin{aligned}
\partial A_j^{(1/2)}/\partial t &= -(1-m^2)q_0^2\{[-1 + (2i\boldsymbol{q}_j^0\cdot\boldsymbol{\nabla}_s)^2]A_j^{(1/2)} + [3n_0^{(1/2)^2} \\
&\quad + 2g_2 n_0^{(1/2)} + g\psi_0^{(1/2)^2}]A_j^{(1/2)} + 3A_j^{(1/2)}\Big[|A_j^{(1/2)}|^2 \\
&\quad + 2\sum_{k,l\neq j}^{k<l}(|A_k^{(1/2)}|^2 + |A_l^{(1/2)}|^2)\Big] + (6n_0^{(1/2)} \\
&\quad + 2g_2)\sum_{k,l\neq j}^{k<l} A_k^{(1/2)^*}A_l^{(1/2)^*} - 2\alpha_0[\psi_0^{(1/2)} \\
&\quad \times(2i\boldsymbol{q}_j^0\cdot\boldsymbol{\nabla}_s)A_j^{(1/2)} + (2i\boldsymbol{q}_j^0\cdot\boldsymbol{\nabla}_s)(\psi_0^{(1/2)}A_j^{(1/2)})]\}, \quad (47)
\end{aligned}$$

$$\partial n_0^{(1/2)}/\partial t = q_0^4\nabla_s^2 n_0^{(1/2)}, \quad (48)$$

$$\partial\psi_0^{(1/2)}/\partial t = mq_0^4\nabla_s^2\psi_0^{(1/2)}. \quad (49)$$

Using the scaling relation $A_j=\epsilon^{1/2}A_j^{(1/2)}$, $n_0=\epsilon^{1/2}n_0^{(1/2)}$, and $\psi_0=\epsilon^{1/2}\psi_0^{(1/2)}$, we can then obtain the corresponding amplitude equations in the unscaled units (x,y,t).

It is noted that the direct solutions to Eq. (46) have the form

$$n^{(3/2)} = n_0^{(3/2)}(X,Y,T) + \sum_{j=1}^{3} A_j^{(3/2)}(X,Y,T)e^{i\boldsymbol{q}_j^0\cdot\boldsymbol{r}} + \text{c.c.} + \text{higher harmonics}, \quad (50)$$

$$\psi^{(3/2)} = \psi_0^{(3/2)}(X,Y,T) + \sum_{j=1}^{3} \psi_j^{(3/2)}(X,Y,T)e^{i\boldsymbol{q}_j^0\cdot\boldsymbol{r}} + \text{c.c.} + \text{higher harmonics}. \quad (51)$$

Compared to Eq. (45) for the $\mathcal{O}(\epsilon^{1/2})$ and $\mathcal{O}(\epsilon)$ solutions, it can be found that the complex amplitudes ψ_j corresponding to the periodic modes of the concentration field in substitutional binary alloys considered here is generally of order ϵ higher than A_j, n_0, and ψ_0. For systems in which a sublattice ordering occurs (such as B2 or B32 ordering in bcc crystals), ψ_j would be of the same order as these other fields. To describe sublattice ordering a different free energy functional from the one given in Eq. (41) would also be required. Detailed results will be presented elsewhere.

B. A hybrid approach: Full order amplitude equations

The lowest order amplitude Eqs. (47)–(49) derived above are not sufficient to describe the evolution of binary systems;

e.g., Eq. (47) for A_j is not rotationally invariant, and Eqs. (48) and (49) for n_0 and ψ_0 are just diffusion equations and would lead to a steady state solution of constant n_0 and ψ_0 values at long enough time. We thus need higher-order amplitude equations, which in principle can be derived by extending the multiple-scale process described above to higher-order expansions. However, the procedure is complicated and tedious. In the following we use, instead, a simplified approach combining the above steps of multiple-scale expansion and the idea of the "Quick and Dirty" RG method [26,27].

The first step is the standard multiple-scale expansion given in Sec. III A, starting from the scale separation Eq. (42). From the solution forms of Eqs. (45), (50), and (51), we know that to all orders of ϵ the solutions of n and ψ fields can be written as

$$n = n_0(X,Y,T) + \sum_{j=1}^{3} A_j(X,Y,T)e^{i\mathbf{q}_j^0\cdot\mathbf{r}} + \text{c.c.} + \text{higher harmonics}, \tag{52}$$

$$\psi = \psi_0(X,Y,T) + \sum_{j=1}^{3} \psi_j(X,Y,T)e^{i\mathbf{q}_j^0\cdot\mathbf{r}} + \text{c.c.} + \text{higher harmonics}, \tag{53}$$

with (X,Y,T) the slow scales. Thus, based on the separation between "fast"/"slow" scales the following expansions (full-order) can be obtained,

$$\nabla^2 n \to \epsilon\nabla_s^2 n_0 + \sum_{j=1}^{3} (\mathcal{L}_j^s A_j)e^{i\mathbf{q}_j^0\cdot\mathbf{r}} + \text{c.c.} + \{\cdots\},$$

$$(\nabla^2 + q_0^2)^2 n \to (\epsilon\nabla_s^2 + q_0^2)^2 n_0 + \sum_{j=1}^{3} (\mathcal{G}_j^{s2} A_j)e^{i\mathbf{q}_j^0\cdot\mathbf{r}} + \text{c.c.} + \{\cdots\},$$

$$(\nabla^2 + \nabla^4)(n\psi) \to (\epsilon\nabla_s^2 + \epsilon^2\nabla_s^4)\left(n_0\psi_0 + \sum_{j=1}^{3} A_j\psi_j^* + \text{c.c.}\right) + \sum_{j=1}^{3}\left[\mathcal{L}_j^s\mathcal{G}_j^s\left(\psi_0 A_j + n_0\psi_j + \sum_{k,l\neq j}^{k<l} A_k^*\psi_l^*\right)\right]e^{i\mathbf{q}_j^0\cdot\mathbf{r}} + \text{c.c.} + \{\cdots\},$$

$$n^2 \to n_0^2 + 2\sum_{j=1}^{3}|A_j|^2 + \sum_{j=1}^{3}\left(2n_0 A_j + 2\sum_{k,l\neq j}^{k<l} A_k^* A_l^*\right)e^{i\mathbf{q}_j^0\cdot\mathbf{r}} + \text{c.c.} + \{\cdots\},$$

$$n^3 \to n_0^3 + 6n_0\sum_{j=1}^{3}|A_j|^2 + 6\left(\prod_{j=1}^{3} A_j + \text{c.c.}\right) + \sum_{j=1}^{3}\left\{3(n_0^2 + |A_j|^2)A_j + 6\sum_{k,l\neq j}^{k<l}[n_0 A_k^* A_l^* + A_j(|A_k|^2 + |A_l|^2)]\right\}e^{i\mathbf{q}_j^0\cdot\mathbf{r}} + \text{c.c.} + \{\cdots\},$$

$$n\psi^2 \to n_0\psi_0^2 + 2n_0\sum_{j=1}^{3}|\psi_j|^2 + \sum_{j=1}^{3}\left(2\psi_0 A_j + \sum_{k\neq l\neq j} A_k^*\psi_l^*\right)\psi_j^* + \text{c.c.} + \sum_{j=1}^{3}\left[2n_0\left(\psi_0\psi_j + \sum_{k,l\neq j}^{k<l}\psi_k^*\psi_l^*\right) + \left(\psi_0^2 + 2\sum_{k=1}^{3}|\psi_k|^2\right)A_j + 2\psi_0\sum_{k\neq l\neq j} A_k^*\psi_l^* + 2\psi_j\sum_{k\neq j}(A_k\psi_k^* + \text{c.c.}) + A_j^*\psi_j^2\right]e^{i\mathbf{q}_j^0\cdot\mathbf{r}} + \text{c.c.} + \{\cdots\},$$

$$\cdots\cdots \tag{54}$$

where $\{\cdots\}$ refers to the contributions from higher harmonics and the slow operators are given by

$$\mathcal{L}_j^s = \epsilon\nabla_s^2 + \epsilon^{1/2}(2i\mathbf{q}_j^0\cdot\boldsymbol{\nabla}_s) - q_0^2,$$

$$\mathcal{G}_j^s = \mathcal{L}_j^s + q_0^2 = \epsilon\nabla_s^2 + \epsilon^{1/2}(2i\mathbf{q}_j^0\cdot\boldsymbol{\nabla}_s). \tag{55}$$

Assuming that higher harmonic terms can be neglected, the binary PFC Eqs. (38) and (39) are then replaced by

$$\epsilon\partial_T n_0 + \epsilon\sum\nolimits_j \partial_T A_j e^{i\mathbf{q}_j^0\cdot\mathbf{r}} + \text{c.c.} = \mathcal{D}_1^s + m\mathcal{D}_2^s, \tag{56}$$

$$\epsilon\partial_T\psi_0 + \epsilon\sum\nolimits_j \partial_T\psi_j e^{i\mathbf{q}_j^0\cdot\mathbf{r}} + \text{c.c.} = m\mathcal{D}_1^s + \mathcal{D}_2^s, \tag{57}$$

where $\mathcal{D}_1^s$ and $\mathcal{D}_2^s$ are the corresponding expansion of $\mathcal{D}_1$ and $\mathcal{D}_2$, as obtained by substituting Eq. (54) into Eq. (39). Integrating Eqs. (56) and (57) over the eigenmodes $\int d\mathbf{r}\{e^{-i\mathbf{q}_j^0\cdot\mathbf{r}}, 1\}$, keeping in mind that "fast" and "slow" scales are separated, and in the final step returning to original unscaled units (x,y,t), we arrive at the following full-order amplitude equations for the binary PFC model:

$$\partial n_0/\partial t = \nabla^2\frac{\delta\mathcal{F}}{\delta n_0} + m\nabla^2\frac{\delta\mathcal{F}}{\delta\psi_0}, \tag{58}$$

$$\partial A_j/\partial t = \mathcal{L}_j\left(\frac{\delta\mathcal{F}}{\delta A_j^*} + m\frac{\delta\mathcal{F}}{\delta\psi_j^*}\right) \simeq -q_0^2\left(\frac{\delta\mathcal{F}}{\delta A_j^*} + m\frac{\delta\mathcal{F}}{\delta\psi_j^*}\right), \tag{59}$$

$$\partial\psi_0/\partial t = m\nabla^2\frac{\delta\mathcal{F}}{\delta n_0} + \nabla^2\frac{\delta\mathcal{F}}{\delta\psi_0}, \tag{60}$$

$$\partial\psi_j/\partial t = \mathcal{L}_j\left(m\frac{\delta\mathcal{F}}{\delta A_j^*} + \frac{\delta\mathcal{F}}{\delta\psi_j^*}\right) \simeq -q_0^2\left(m\frac{\delta\mathcal{F}}{\delta A_j^*} + \frac{\delta\mathcal{F}}{\delta\psi_j^*}\right), \tag{61}$$

where $j=1,2,3$, and

$$\begin{aligned}\mathcal{F} = \int d\boldsymbol{r}\Bigg\{ & -\frac{1}{2}\epsilon n_0^2 + \frac{1}{2}[(\nabla^2+q_0^2)n_0]^2 + \frac{1}{3}g_2 n_0^3 + \frac{1}{4}n_0^4 + (-\epsilon + 3n_0^2 + 2g_2 n_0 + g\psi_0^2)\sum_{j=1}^{3}|A_j|^2 + \sum_{j=1}^{3}|\mathcal{G}_j A_j|^2 + \frac{3}{2}\sum_{j=1}^{3}|A_j|^4 \\ & + (6n_0+2g_2)\left(\prod_{j=1}^{3}A_j + \text{c.c.}\right) + 6\sum_{j<k}|A_j|^2|A_k|^2 + g\Bigg[\frac{1}{2}n_0^2\psi_0^2 + n_0^2\sum_{j=1}^{3}|\psi_j|^2 + 2\sum_{j,k=1}^{3}|A_j|^2|\psi_k|^2 + \sum_{j=1}^{3}\left(2n_0\psi_0 A_j\psi_j^* + \frac{1}{2}A_j^2\psi_j^{*2} + \text{c.c.}\right) \\ & + \sum_{j\neq k}(A_j\psi_j^* + \text{c.c.})(A_k\psi_k^* + \text{c.c.}) + \sum_{j\neq k\neq l}(n_0\psi_j^* + \psi_0 A_j^*)A_k^*\psi_l^* + \text{c.c.}\Bigg] + 2\alpha_0\Bigg[\psi_0 n_0(\nabla^2+\nabla^4)n_0 + \psi_0\left(\sum_{j=1}^{3}A_j^*\mathcal{L}_j\mathcal{G}_j A_j + \text{c.c.}\right) \\ & + n_0(\nabla^2+\nabla^4)\left(\sum_{j=1}^{3}A_j\psi_j^* + \text{c.c.}\right) + n_0\sum_{j=1}^{3}\psi_j^*\mathcal{L}_j\mathcal{G}_j A_j + \sum_{j\neq k\neq l}A_j\psi_k\mathcal{L}_l\mathcal{G}_l A_l + \text{c.c.}\Bigg] + \frac{1}{2}w_0\psi_0^2 + \frac{1}{2}K_0|\nabla\psi_0|^2 \\ & + \frac{1}{4}u_0\psi_0^4 + (w_0+3u_0\psi_0^2)\sum_{j=1}^{3}|\psi_j|^2 - \frac{1}{2}K_0\sum_{j=1}^{3}(\psi_j\mathcal{L}_j^*\psi_j^* + \text{c.c.}) + u_0\Bigg[\frac{3}{2}\sum_{j=1}^{3}|\psi_j|^4 + 6\psi_0\left(\prod_{j=1}^{3}\psi_j + \text{c.c.}\right) + 6\sum_{j<k}|\psi_j|^2|\psi_k|^2\Bigg] \\ & + v_1\Bigg[n_0\psi_0^2 + 2n_0\sum_{j=1}^{3}|\psi_j|^2 + 2\psi_0\left(\sum_{j=1}^{3}A_j\psi_j^* + \text{c.c.}\right) + \sum_{j\neq k\neq l}A_j\psi_k\psi_l + \text{c.c.}\Bigg]\Bigg\}. \end{aligned} \tag{62}$$

Corresponding to Eq. (55), the operators $\mathcal{L}_j$ and $\mathcal{G}_j$ (in the original scales) are defined by

$$\mathcal{L}_j = \nabla^2 + 2i\boldsymbol{q}_j^0\cdot\boldsymbol{\nabla} - q_0^2, \quad \mathcal{G}_j = \mathcal{L}_j + q_0^2 = \nabla^2 + 2i\boldsymbol{q}_j^0\cdot\boldsymbol{\nabla}, \tag{63}$$

and for simplicity, in Eqs. (59)–(62) the operator $\mathcal{L}_j$ can be replaced by $-q_0^2$ in the long wavelength approximation as adopted in Ref. [32].

As discussed at the end of Sec. III A, the amplitudes ψ_j are of $\mathcal{O}(\epsilon)$ higher compared to the others for the free energy functional considered here. Thus the above amplitude equations can be further simplified by assuming $\psi_j \sim 0$, which leads to

$$\begin{aligned}\partial A_j/\partial t = & -q_0^2\frac{\delta\mathcal{F}}{\delta A_j^*} - mq_0^2\Bigg\{2\alpha_0\Bigg[A_j(\nabla^2+\nabla^4)n_0 + n_0\mathcal{L}_j\mathcal{G}_j A_j \\ & + \sum_{k\neq l\neq j}A_k^*\mathcal{L}_l^*\mathcal{G}_l^* A_l^*\Bigg] + 2g\psi_0\left(n_0 A_j + \sum_{k,l\neq j}^{k<l}A_k^* A_l^*\right) \\ & + 2v_1\psi_0 A_j\Bigg\} = -q_0^2\frac{\delta\mathcal{F}}{\delta A_j^*} - mq_0^2\left.\frac{\delta\mathcal{F}}{\delta\psi_j^*}\right|_{\psi_j=0}.\end{aligned}$$

The dynamic equations for n_0 and ψ_0 are still governed by Eqs. (58) and (60). The amplitude equations can be further simplified by noting from Eq. (61) $0 \simeq \partial\psi_j/\partial t = -q_0^2(m\delta\mathcal{F}/\delta A_j^* + \delta\mathcal{F}/\delta\psi_j^*|_{\psi_j=0})$. Thus, the above dynamic equation for A_j can be further approximated as

$$\partial A_j/\partial t \simeq -q_0^2(1-m^2)\frac{\delta\mathcal{F}}{\delta A_j^*}, \tag{64}$$

which to lowest order recovers the result of multiple-scale approach given in Eq. (47). In the applications that will be examined in Sec. V the simplified amplitude Eqs. (58), (60), and (64) will be used.

IV. NOISE DYNAMICS AND STOCHASTIC AMPLITUDE EQUATIONS

In the original PFC model [23,24] a conserved noise dynamics has been incorporated. However, in DDFT it has been argued that the dynamic equation governing the density field evolution should be deterministic and an additional stochastic noise term added to Eq. (1) would lead to an artificial double-counting of thermal fluctuations [76]. On the other hand, recent studies [87] have shown that deterministic DDFT dynamics governs the ensemble averaged density field $\rho(\boldsymbol{r},t)$, while if the density field is temporally coarse grained—as is the assumption in PFC modeling—the corresponding dynamic equation would then be stochastic, but with a (unknown) coarse-grained free energy functional instead of the equilibrium Helmholtz free energy functional used in static DFT. In the current case of PFC modeling, quite drastic approximations have been made to the DFT free energy functional [particularly at the level of the direct correlation functions; see e.g., Eqs. (3), (4), and (18)], and hence it could be argued that the incorporation of noise terms in the PFC dynamics would be necessary and useful to capture the qualitative effects of fluctuations in phenomena such as ho-

mogeneous nucleation. In what follows, noise will be added to the PFC models studied above and the corresponding stochastic amplitude equations will be derived for both single-component and binary systems.

A. Single-component PFC

The stochastic DDFT equation for single-component systems is given by Eq. (1) with a multiplicative noise term $\nabla\cdot[\sqrt{\rho(\boldsymbol{r},t)}\boldsymbol{\zeta}(\boldsymbol{r},t)]$ added to the right-hand-side, where the noise field $\boldsymbol{\zeta}(\boldsymbol{r},t)$ is determined by (with $\Gamma_0=2k_BTM$)

$$\langle\boldsymbol{\zeta}(\boldsymbol{r},t)\rangle=0,$$

$$\langle\zeta^{\mu}(\boldsymbol{r},t)\zeta^{\nu}(\boldsymbol{r}',t')\rangle=\Gamma_0\delta(\boldsymbol{r}-\boldsymbol{r}')\delta(t-t')\delta^{\mu\nu}\quad(\mu,\nu=x,y,z). \tag{65}$$

The corresponding dynamic equation governing the rescaled density field n is similar to Eq. (7), i.e., $\partial n/\partial t=M'\nabla\cdot[(1+n)\nabla\delta\mathcal{F}/\delta n]+\nabla\cdot[\sqrt{(1+n)/\rho_l}\boldsymbol{\zeta}]$. Adopting the lowest order approximation as given in Sec. II A, we can write the rescaled stochastic PFC equation as

$$\partial n/\partial t=\nabla^2[-\epsilon n+(\nabla^2+q_0^2)^2n+g_2n^2+n^3]+\nabla\cdot\boldsymbol{\zeta}, \tag{66}$$

where the rescaled noise $\boldsymbol{\zeta}$ is also determined by Eq. (65) but with $\Gamma_0=2v/(B^{x2}R^d\rho_l)$ (where d is the dimensionality).

To derive the associated stochastic amplitude equations, we follow the standard multiple-scale approach in the limit of small ϵ, which leads to the expansion of density field n in terms of the zeroth-mode average density n_0 and complex amplitudes A_j that are varying on slow scales (X,Y,T); see Eq. (52). Effects of external noise can be approximated via a projection procedure used in hydrodynamic analysis [88,89]. Based on the fact that thermal noises originate from the fluctuations or random motion of individual atoms/molecules at the microscopic scales, we can project $\boldsymbol{\zeta}$ onto the base modes given in Eq. (52), i.e.,

$$\boldsymbol{\zeta}=\boldsymbol{\zeta}_0(X,Y,T)+\sum_{j=1}^{3}\boldsymbol{\zeta}_{A_j}(X,Y,T)e^{i\boldsymbol{q}_j^0\cdot\boldsymbol{r}}+\text{c.c.}, \tag{67}$$

where

$$\langle\boldsymbol{\zeta}_0\rangle=\langle\boldsymbol{\zeta}_{A_j}\rangle=0,\quad\langle\boldsymbol{\zeta}_{A_i}\boldsymbol{\zeta}_{A_j}\rangle=\langle\boldsymbol{\zeta}_0\boldsymbol{\zeta}_{A_j}\rangle=\langle\boldsymbol{\zeta}_0\boldsymbol{\zeta}_{A_j}^*\rangle=0,$$

$$\langle\zeta_0^{\mu}\zeta_0^{\nu}\rangle=\vartheta_0\Gamma_0\delta(\boldsymbol{r}-\boldsymbol{r}')\delta(t-t')\delta^{\mu\nu},$$

$$\langle\zeta_{A_i}^{\mu}\zeta_{A_j}^{\nu\,*}\rangle=\vartheta_i\Gamma_0\delta(\boldsymbol{r}-\boldsymbol{r}')\delta(t-t')\delta_{ij}\delta^{\mu\nu}, \tag{68}$$

(with $i,j=1,2,3$; $\mu,\nu=x,y$). Here ϑ_i $(i=0,1,2,3)$ is a constant determining the noise correlation strength, which can be approximated as $\vartheta_i=\vartheta=1/7$ if equal contribution from all modes in Eq. (67) is assumed. Thus the random noise term in Eq. (66) is given by

$$\nabla\cdot\boldsymbol{\zeta}=\sum_{j=1}^{3}i\boldsymbol{q}_j^0\cdot\boldsymbol{\zeta}_{A_j}e^{i\boldsymbol{q}_j^0\cdot\boldsymbol{r}}+\text{c.c.}+\epsilon^{1/2}\Bigg[\partial_X\zeta_0^x+\partial_Y\zeta_0^y+\sum_{j=1}^{3}(\partial_X\zeta_{A_j}^x+\partial_Y\zeta_{A_j}^y)e^{i\boldsymbol{q}_j^0\cdot\boldsymbol{r}}+\text{c.c.}\Bigg]. \tag{69}$$

In order to be relevant in the amplitude expansion, it is necessary that $\nabla\cdot\boldsymbol{\zeta}\sim\mathcal{O}(\epsilon^{3/2})$, leading to $\boldsymbol{\zeta}_{A_j}\sim\mathcal{O}(\epsilon^{3/2})$ and hence the noise intensity $\Gamma_0\sim\mathcal{O}(\epsilon)$. The latter yields $\boldsymbol{\zeta}_0\sim\mathcal{O}(\epsilon^{3/2})$, which can be deduced from Eq. (68).

Following the procedure of multiple-scale expansion and retaining the random force contribution to the lowest order, we can derive the following stochastic amplitude equations:

$$\partial A_j/\partial t=-q_0^2\delta\mathcal{F}/\delta A_j^*+\zeta_j, \tag{70}$$

$$\partial n_0/\partial t=\nabla^2\delta\mathcal{F}/\delta n_0+\nabla\cdot\boldsymbol{\zeta}_0, \tag{71}$$

where $\mathcal{F}$ is the effective free energy of the single-component amplitude representation (see Refs. [3,30,37] for the detailed form), which is given by Eq. (62) with ψ_0 and ψ_j set to 0. Also, $\zeta_j=i\boldsymbol{q}_j^0\cdot\boldsymbol{\zeta}_{A_j}$ $(j=1,2,3)$ and

$$\langle\zeta_j\rangle=\langle\boldsymbol{\zeta}_0\rangle=0,$$

$$\langle\zeta_i\zeta_j\rangle=\langle\boldsymbol{\zeta}_0\zeta_j\rangle=\langle\boldsymbol{\zeta}_0\zeta_j^*\rangle=0,$$

$$\langle\zeta_i\zeta_j^*\rangle=\vartheta_iq_0^2\Gamma_0\delta(\boldsymbol{r}-\boldsymbol{r}')\delta(t-t')\delta_{ij}, \tag{72}$$

$$\langle\zeta_0^{\mu}\zeta_0^{\nu}\rangle=\vartheta_0\Gamma_0\delta(\boldsymbol{r}-\boldsymbol{r}')\delta(t-t')\delta^{\mu\nu}.$$

The noise dynamics is then consistent with the dynamics of amplitude representation, i.e., nonconserved dynamics for A_j in Eq. (70) and conserved one for n_0 in Eq. (71).

B. Binary PFC

Similar to the single-component system, based on Eq. (15) the stochastic DDFT equations for a binary system can be written as

$$\frac{\partial\rho_A}{\partial t}=\nabla\cdot\left[M_A\rho_A\nabla\frac{\delta\mathcal{F}}{\delta\rho_A}+\sqrt{\rho_A}\boldsymbol{\zeta}_A\right],$$

$$\frac{\partial\rho_B}{\partial t}=\nabla\cdot\left[M_B\rho_B\nabla\frac{\delta\mathcal{F}}{\delta\rho_B}+\sqrt{\rho_B}\boldsymbol{\zeta}_B\right], \tag{73}$$

where for noises $(\alpha,\beta=A,B;\ \mu,\nu=x,y,z;\ \Gamma_\alpha=2k_BTM_\alpha)$,

$$\langle\boldsymbol{\zeta}_i(\boldsymbol{r},t)\rangle=0,\quad\langle\zeta_\alpha^{\mu}(\boldsymbol{r},t)\zeta_\beta^{\nu}(\boldsymbol{r}',t')\rangle=\Gamma_\alpha\delta(\boldsymbol{r}-\boldsymbol{r}')\delta(t-t')\delta_{\alpha\beta}\delta^{\mu\nu}. \tag{74}$$

From Eqs. (19) and (26) the dynamics equations for n and ψ fields can be rewritten as

$$\partial n/\partial t = M_1\mathcal{D}_1 + M_2\mathcal{D}_2 + \nabla\cdot[\sqrt{1+n}(\sqrt{1+\psi}\zeta_A + \sqrt{1-\psi}\zeta_B)],$$

$$\partial\psi/\partial t = \frac{1}{1+n}\{(M_2 - M_1\psi)\mathcal{D}_1 + (M_1 - M_2\psi)\mathcal{D}_2 + (1-\psi)\nabla\cdot[\sqrt{(1+n)(1+\psi)}\zeta_A] - (1+\psi)\nabla\cdot[\sqrt{(1+n)(1-\psi)}\zeta_B]\}, \quad (75)$$

where we have rescaled $\zeta_{A(B)} \to \zeta_{A(B)}/\sqrt{2\rho_l}$. Following the procedure given in Sec. II B and only retaining the lowest order noise terms, we can derive the rescaled stochastic binary PFC equations as

$$\partial n/\partial t = \mathcal{D}_1 + m\mathcal{D}_2 + \nabla\cdot\zeta_n, \quad \partial\psi/\partial t = m\mathcal{D}_1 + \mathcal{D}_2 + \nabla\cdot\zeta_\psi, \quad (76)$$

where the expressions of $\mathcal{D}_1$ and $\mathcal{D}_2$ have been given in Eqs. (39)–(41). The noise terms are defined by

$$\zeta_n = \zeta_A + \zeta_B, \quad \zeta_\psi = \zeta_A - \zeta_B, \quad (77)$$

where $\zeta_{A(B)}$ also obeys Eq. (74), although with $\Gamma_\alpha = k_BTM_\alpha\upsilon/(M_1B_0^{x2}R^d\rho_l)$ due to the rescaling, and

$$\langle\zeta_n\rangle = \langle\zeta_\psi\rangle = 0, \quad \langle\zeta_n^\mu\zeta_\psi^\nu\rangle = (\Gamma_A - \Gamma_B)\delta(\mathbf{r}-\mathbf{r}')\delta(t-t')\delta^{\mu\nu},$$

$$\langle\zeta_n^\mu\zeta_n^\nu\rangle = \langle\zeta_\psi^\mu\zeta_\psi^\nu\rangle = (\Gamma_A + \Gamma_B)\delta(\mathbf{r}-\mathbf{r}')\delta(t-t')\delta^{\mu\nu}, \quad (78)$$

with $\Gamma_A+\Gamma_B = 2\upsilon/(B_0^{x2}R^d\rho_l)$ and $\Gamma_A-\Gamma_B = m(\Gamma_A+\Gamma_B) = 2m\upsilon/(B_0^{x2}R^d\rho_l)$.

Using the multiple-scale approach, we can expand the density field n according to Eq. (52) while assuming the concentration field as slowly varying, $\psi=\psi_0(X,Y,T)$ [that is, keeping only the zeroth mode and neglecting the higher-order contributions from ψ_j in Eq. (53), as discussed in Sec. III B]. Similar to the single-component case, the projection of noises can be given by

$$\zeta_n = \zeta_0(X,Y,T) + \sum_{j=1}^{3}\zeta_{A_j}(X,Y,T)e^{i\mathbf{q}_j^0\cdot\mathbf{r}} + \text{c.c.}, \quad \zeta_\psi = \zeta_\psi(X,Y,T). \quad (79)$$

Thus the expression of $\nabla\cdot\zeta_n$ is the same as Eq. (69), while $\nabla\cdot\zeta_\psi = \epsilon^{1/2}(\partial_X\zeta_\psi^x + \partial_Y\zeta_\psi^y)$. Also we can estimate $\zeta_{A_j}, \zeta_0, \zeta_\psi \sim \mathcal{O}(\epsilon^{3/2})$ and $\Gamma_A, \Gamma_B \sim \mathcal{O}(\epsilon)$.

The stochastic amplitude equations for binary PFC model can then be derived, i.e.,

$$\partial A_j/\partial t = -q_0^2(1-m^2)\frac{\delta\mathcal{F}}{\delta A_j^*} + \zeta_j, \quad (80)$$

$$\partial n_0/\partial t = \nabla^2\frac{\delta\mathcal{F}}{\delta n_0} + m\nabla^2\frac{\delta\mathcal{F}}{\delta\psi_0} + \nabla\cdot\zeta_0, \quad (81)$$

$$\partial\psi_0/\partial t = m\nabla^2\frac{\delta\mathcal{F}}{\delta n_0} + \nabla^2\frac{\delta\mathcal{F}}{\delta\psi_0} + \nabla\cdot\zeta_{\psi_0}, \quad (82)$$

where the deterministic parts have been obtained in Sec. III B; see Eqs. (58), (60), and (64), as well as Eq. (62) for the effective potential $\mathcal{F}$. For the noise terms, $\zeta_j = i\mathbf{q}_j^0\cdot\zeta_{A_j}$ $(j=1,2,3)$, and

$$\langle\zeta_j\rangle = \langle\zeta_0\rangle = \langle\zeta_{\psi_0}\rangle = 0,$$

$$\langle\zeta_i\zeta_j\rangle = \langle\zeta_0\zeta_j\rangle = \langle\zeta_0\zeta_j^*\rangle = \langle\zeta_{\psi_0}\zeta_j\rangle = \langle\zeta_{\psi_0}\zeta_j^*\rangle = 0,$$

$$\langle\zeta_i\zeta_j^*\rangle = \vartheta_i q_0^2(\Gamma_A+\Gamma_B)\delta(\mathbf{r}-\mathbf{r}')\delta(t-t')\delta_{ij},$$

$$\langle\zeta_0^\mu\zeta_0^\nu\rangle = \vartheta_0(\Gamma_A+\Gamma_B)\delta(\mathbf{r}-\mathbf{r}')\delta(t-t')\delta^{\mu\nu},$$

$$\langle\zeta_{\psi_0}^\mu\zeta_{\psi_0}^\nu\rangle = (\Gamma_A+\Gamma_B)\delta(\mathbf{r}-\mathbf{r}')\delta(t-t')\delta^{\mu\nu},$$

$$\langle\zeta_{\psi_0}^\mu\zeta_0^\nu\rangle = (\Gamma_A-\Gamma_B)\delta(\mathbf{r}-\mathbf{r}')\delta(t-t')\delta^{\mu\nu}, \quad (83)$$

with $i,j=1,2,3$ and $\mu,\nu=x,y$. If assuming $\Gamma_A \simeq \Gamma_B$ (for equal mobility $M_A \simeq M_B$ and $m\simeq 0$), i.e., with almost the same noise/fluctuation intensity for A and B components, we have $\langle\zeta_{\psi_0}^\mu\zeta_0^\nu\rangle \simeq 0$ and hence all noise terms $(\zeta_j, \zeta_0, \zeta_{\psi_0})$ can be treated independently. However, for the case of different mobilities $(M_A \neq M_B$ and $m\neq 0)$, we get $\langle\zeta_{\psi_0}^\mu\zeta_0^\nu\rangle \neq 0$, and hence noises ζ_0 and ζ_{ψ_0} for 0th-mode density fields n_0 and ψ_0 are then correlated. Similar results can be obtained for noises ζ_n and ζ_ψ in the stochastic PFC Eqs. (75) and (78).

V. APPLICATIONS IN ALLOY HETEROSTRUCTURES

As discussed in the introduction, the PFC model and the corresponding amplitude equations have applied to the study of a wide variety of phenomena involved in material processing and microstructure evolution. In this section we will illustrate how the amplitude equations derived in the preceding sections can be employed to examine the effect of surface segregation and alloy intermixing. Alloy intermixing is known to play an important role in the growth and processing of material heterostructures, including morphological and compositional profiles and the associated sample optoelectronic properties and functionality. Recent intensive studies on thin film epitaxy and atomic deposition have shown the important effects of intermixing on nanostructure self-assembly. Typical examples include InAs(InGaAs)/GaAs(001) [66–68] or Ge(SiGe)/Si(001) [69,70] heteroepitaxy that has been investigated extensively (particularly the intermixing-caused alloying of wetting layers and quantum dots), and the interlayer diffusion in semiconductor multilayers or superlattices such as InP/InGaAs [71], GaAs/GaSb [72], and GaAs/InAs [73]. An important phenomenon in these epitaxial layers is the occurrence of surface segregation, in which an enrichment of one of the film components at a surface or interface region occurs. This has been observed in a variety of material systems including III-V and II-VI semiconductor heterostructures [66–73]. To address these complicated phenomena and effects, the basic processes and mechanisms of intra- and interlayer diffusion at nearly planar interfaces as well as their coupling with material processing and growth parameters needs to be clarified.

In light of the above observations, the focus of this section is on heterostructures of a nearly planar interface, for

both lattice-matched and strained epitaxial layers. For layers stressed due to lattice mismatch, the configurations studied here are metastable in nature, and our results will be used for further studies of the associated later-stage nanostructure evolution (e.g., quantum dots), which will be presented elsewhere. For such film geometry with a planar interface, it can be assumed that both morphological and compositional profiles along the lateral direction are approximately uniform or homogeneous (at least metastability), and hence these structural profiles vary only along the direction (y) normal to the interface. An advantage of the amplitude equation representation of the PFC model developed above is that the system of interest can then be mapped onto an effective one-dimensional (1D) description, as will be shown below.

A. Effective 1D model system with elasticity

To address the elasticity incorporated in the amplitude equation formalism, it is useful to note that the structural amplitudes can be written as

$$A_j = A_j' e^{i\boldsymbol{q}_j^0\cdot\boldsymbol{u}} \quad (j=1,2,3), \tag{84}$$

where for 2D hexagonal structure $\boldsymbol{q}_j^0$ are the three basic wave vectors given in Sec. III and $\boldsymbol{u}=\delta_0(x\hat{x}+y\hat{y})$ describes the bulk compression or dilation. The effective free energy $\mathcal{F}$ in Eq. (62) can be rewritten as (neglecting the higher-order contributions from ψ_j and approximating $\mathcal{L}_j \simeq -q_0^2$)

$$\begin{aligned}\mathcal{F} = \int d\boldsymbol{r}\Bigg\{ & -\frac{1}{2}\epsilon n_0^2 + \frac{1}{2}[(\nabla^2+q_0^2)n_0]^2 + \frac{1}{3}g_2 n_0^3 + \frac{1}{4}n_0^4 \\ & + (-\epsilon + 3n_0^2 + 2g_2 n_0 + g\psi_0^2)\sum_j |A_j'|^2 + \sum_j |\mathcal{G}_j' A_j'|^2 \\ & + \frac{3}{2}\sum_j |A_j'|^4 + (6n_0+2g_2)\left(\prod_j A_j' + \text{c.c.}\right) + 6\sum_{j<k}|A_j'|^2|A_k'|^2 \\ & + \frac{1}{2}w_0\psi_0^2 + \frac{1}{2}K_0|\nabla\psi_0|^2 + \frac{1}{4}u_0\psi_0^4 + \frac{1}{2}g n_0^2\psi_0^2 + v_1 n_0\psi_0^2 \\ & + 2\alpha_0\left[\psi_0 n_0(\nabla^2+\nabla^4)n_0 - q_0^2\psi_0\left(\sum_j A_j'^{*}\mathcal{G}_j' A_j' + \text{c.c.}\right)\right]\Bigg\},\end{aligned} \tag{85}$$

where

$$\mathcal{G}_j' = \nabla^2 + 2i(\boldsymbol{\delta}_j + \boldsymbol{q}_j^0)\cdot\nabla - |\boldsymbol{\delta}_j|^2 - 2\boldsymbol{q}_j^0\cdot\boldsymbol{\delta}_j, \tag{86}$$

with $\delta_1=-\delta_x\hat{x}-\delta_y\hat{y}/2$, $\delta_2=\delta_y\hat{y}$, $\delta_3=\delta_x\hat{x}-\delta_y\hat{y}/2$, $\delta_x=\sqrt{3}q_0\delta_0/2$, and $\delta_y=q_0\delta_0$. The corresponding dynamic equations for A_j', n_0, and ψ_0 are still governed by Eqs. (80)–(82), although with A_j replaced by A_j'. In mechanical equilibrium, we can assume that $A_j' \simeq A$, i.e., $A_j \simeq A\exp(i\boldsymbol{q}_j^0\cdot\boldsymbol{u})$ where A is a constant. Minimizing the effective free energy $\mathcal{F}$ with respect to A yields the equilibrium value $\delta_0^{\text{eq}}=-1+\sqrt{1-2\alpha_0\psi_0} \simeq -\alpha_0\psi_0$ to lowest order. This leads to the equilibrium wave number $q_{\text{eq}}=(1+\delta_0^{\text{eq}})q_0=\sqrt{1-2\alpha_0\psi_0}q_0$ (where α_0 is the rescaled solute expansion coefficient defined in Sec. II B), and the equilibrium amplitude

$$A = \frac{1}{15}\{-(3n_0+g_2) + \sqrt{(3n_0+g_2)^2 - 15[-\epsilon + q_0^4(\delta_0^2+2\delta_0)(\delta_0^2+2\delta_0+4\alpha_0\psi_0) + n_0(3n_0+2g_2) + g\psi_0^2]}\}. \tag{87}$$

The elastic constants (rescaled) are then given by $C_{11}=C_{22}=9A^2$, $C_{12}=C_{44}=C_{11}/3=3A^2$, and Young's modulus $E=8A^2$ [24,25,32].

For the dynamics of a heterostructure configuration with nearly-planar interface (either liquid-solid or solid-solid), we can assume that $A_j'(x,y,t)\simeq A_j^0(y,t)$, $n_0(x,y,t)\simeq n_0^0(y,t)$, and $\psi_0(x,y,t)\simeq\psi_0^0(y,t)$, resulting in an effective 1D description of the system. The dynamics of the amplitude equations then become

$$\partial n_0^0/\partial t = \partial_y^2\frac{\delta\mathcal{F}}{\delta n_0^0} + m\partial_y^2\frac{\delta\mathcal{F}}{\delta\psi_0^0}, \tag{88}$$

$$\partial\psi_0^0/\partial t = m\partial_y^2\frac{\delta\mathcal{F}}{\delta n_0^0} + \partial_y^2\frac{\delta\mathcal{F}}{\delta\psi_0^0}, \tag{89}$$

$$\partial A_j^0/\partial t = -q_0^2(1-m^2)\frac{\delta\mathcal{F}}{\delta A_j^{0*}}, \tag{90}$$

where

$$\begin{aligned}\frac{\delta\mathcal{F}}{\delta n_0^0} = & [-\epsilon + (\partial_y^2+q_0^2)^2]n_0^0 + g_2 n_0^{02} + n_0^{03} + (6n_0^0+2g_2)\sum_j |A_j^0|^2 \\ & + 6\left(\prod_j A_j^0 + \text{c.c.}\right) + (g n_0^0 + v_1)\psi_0^{02} + 2\alpha_0[\psi_0^0(\partial_y^2+\partial_y^4)n_0^0 \\ & + (\partial_y^2+\partial_y^4)(n_0^0\psi_0^0)],\end{aligned} \tag{91}$$

$$\begin{aligned}\frac{\delta\mathcal{F}}{\delta\psi_0^0} = & (w_0 - K_0\partial_y^2)\psi_0^0 + u_0\psi_0^{03} + g\left(n_0^{02} + 2\sum_j |A_j^0|^2\right)\psi_0^0 \\ & + 2v_1 n_0^0\psi_0^0 + 2\alpha_0\Bigg[n_0^0(\partial_y^2+\partial_y^4)n_0^0 - q_0^2\sum_j (A_j^{0*}\mathcal{G}_j^0 A_j^0 \\ & + \text{c.c})\Bigg],\end{aligned} \tag{92}$$

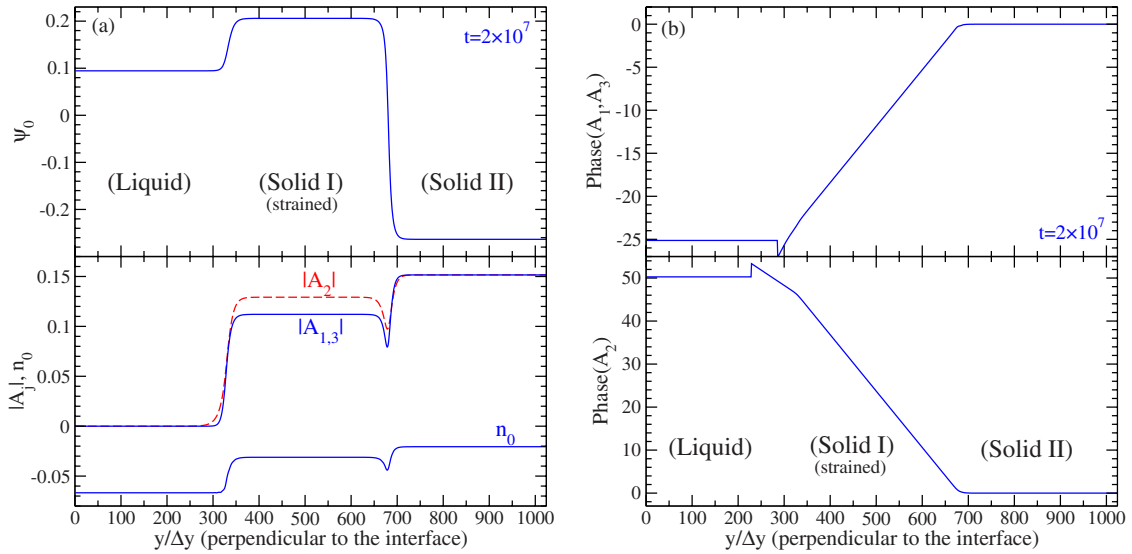

FIG. 1. (Color online) Liquid-solid-solid coexistence profile calculated from the amplitude equations, as characterized by (a) the composition field ψ_0, amplitudes $|A_j|$, and the average density field n_0, and (b) the phases of amplitudes A_j. The parameters are set as $\epsilon=0.02$, $\alpha_0=0.3$, $(g,g_2,u_0,K_0,w_0)=(-1.8,-0.6,4,1,0.008)$, and the time at $t=2\times10^7$. Solid I is strained with respect to the substrate solid II.

$$\frac{\delta\mathcal{F}}{\delta A_j^{0*}} = [-\epsilon + \mathcal{G}_j^{02} + 2g_2 n_0^0 + 3n_0^{02} + g\psi_0^{02}]A_j^0 + 3A_j^0\left[|A_j^0|^2 + 2\sum_{k,l\neq j}^{k<l}(|A_k^0|^2 + |A_l^0|^2)\right] + (6n_0^0 + 2g_2)\prod_{k\neq j} A_k^{0*} - 2\alpha_0 q_0^2[\psi_0^0\mathcal{G}_j^0 A_j^0 + \mathcal{G}_j^0(\psi_0^0 A_j^0)], \tag{93}$$

with

$$\mathcal{G}_j^0 = \partial_y^2 + 2i(\delta_{jy} + q_{jy}^0)\partial_y - |\boldsymbol{\delta}_j|^2 - 2\boldsymbol{q}_j^0\cdot\boldsymbol{\delta}_j. \tag{94}$$

For coherent strained alloy layers, which are of great interest in materials growth, the solid layer is strained with respect to a substrate and subjected to an epitaxial condition $q_x=q_x^{\rm sub}=(\sqrt{3}/2)q_0(1+\delta_0^{\rm sub})$ (with "sub" referring to the substrate). The wavenumber q_y along the vertical or layer growth direction y is determined by the lattice elastic relaxation (or Poisson relaxation in continuum elasticity theory). The system is thus governed by the above amplitude Eqs. (88)–(93), but with δ_0 fixed by the corresponding elasticity quantity $\delta_0^{\rm sub}$ of the substrate (and thus $\delta_x=\sqrt{3}q_0\delta_0^{\rm sub}/2$ and $\delta_y=q_0\delta_0^{\rm sub}$). The vertical strain relaxation (Poisson relaxation) can be determined from the phase of complex amplitudes A_j^0. Furthermore, the misfit strain ε_m of such a solid layer is given by

$$\varepsilon_m = \frac{R_{\rm eq}-R}{R} = \frac{q_x}{q_{x,\rm eq}} - 1 = \frac{\delta_0-\delta_0^{\rm eq}}{1+\delta_0^{\rm eq}}, \tag{95}$$

where R and q_x are lateral lattice spacing and wavenumber of the strained layer, and $R_{\rm eq}$, $q_{x,\rm eq}$, and $\delta_0^{\rm eq}$ are for the corresponding stress-free, equilibrium bulk state.

For the systems studied here the model parameters are chosen such that no phase separation or spinodal decomposition can occur in the bulk of each solid or liquid region. The corresponding conditions on the parameters that assure this are derived via a linear stability analysis of the amplitude equations. Following standard procedures, we substitute the expansion $n_0=\bar{n}_0+\hat{n}_0$, $\psi_0=\bar{\psi}_0+\hat{\psi}_0$, and $A_j=\bar{A}_j+\hat{A}_j$ into Eqs. (58), (60), and (64), obtain the linearized evolution equations for the perturbed quantities $\hat{n}_0$, $\hat{\psi}_0$, and $\hat{A}_j$, and calculate the associated perturbation growth rates. The corresponding results are complicated due to the coupling between the evolution equations of all three perturbed quantities. To estimate the conditions for phase separation, here we simply assume that $\hat{n}_0,\hat{A}_j\sim0$, and only study the stability of concentration field. To first order of $\hat{\psi}_0$ we have

$$\partial\hat{\psi}_0/\partial t \simeq \nabla^2\Big\{-K_0\nabla^2 + w_0 + 3u_0\bar{\psi}_0^2 + g\bar{n}_0^2 + 2v_1\bar{n}_0 + 2g\sum_j|\bar{A}_j|^2 + m[2\alpha_0\bar{n}_0(\nabla^2+\nabla^4) + 2g\bar{n}_0\bar{\psi}_0 + 2v_1\bar{\psi}_0]\Big\}\hat{\psi}_0. \tag{96}$$

In Fourier space, the perturbation growth rate $\sigma(q)$ is then given by

$$\sigma = -q^2[2m\alpha_0\bar{n}_0q^4 + (K_0 - 2m\alpha_0\bar{n}_0)q^2 + w_{\rm eff}], \tag{97}$$

where

$$w_{\rm eff} = w_0 + 3u_0\bar{\psi}_0^2 + g\bar{n}_0^2 + 2v_1\bar{n}_0 + 2g\sum_j|\bar{A}_j|^2 + 2m(g\bar{n}_0 + v_1)\bar{\psi}_0. \tag{98}$$

If $w_{\rm eff}<0$, an instability of the homogeneous alloy occurs,

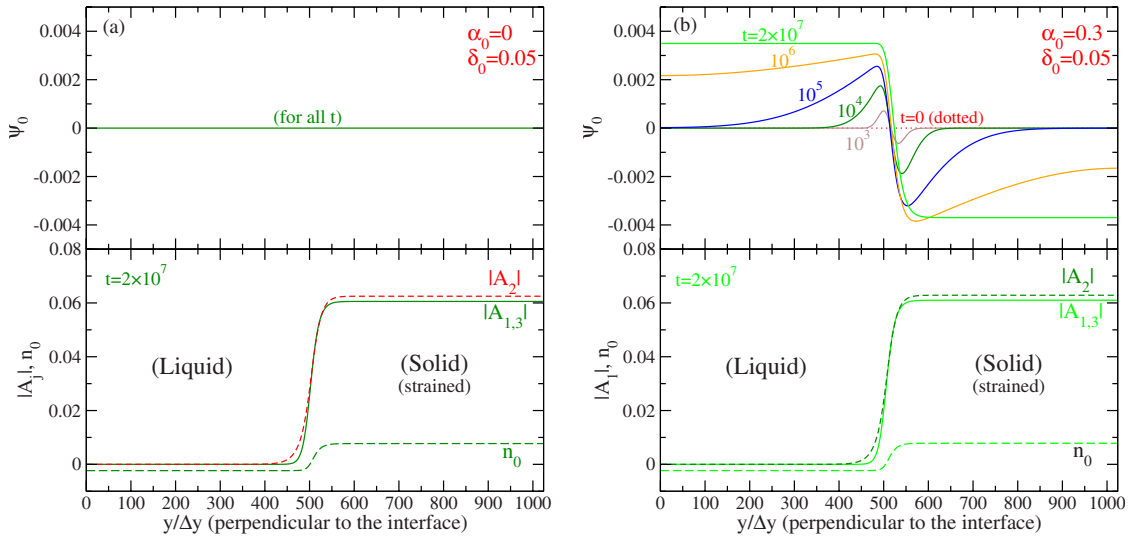

FIG. 2. (Color online) Liquid-solid coexistence profiles, for $\alpha_0=0$ (a) and 0.3 (b). The other parameters are the same as Fig. 1, except for $\epsilon=-0.02$, $w_0=0.088$, and initially $\psi_0=0$. The solid region has a misfit strain of around 5% due to $\delta_0=0.05$ set in the amplitude equations.

leading to spinodal decomposition or phase separation of alloy components. The characteristic wave number (for maximum perturbation growth rate) is then given by $q_{\max}^2=[\sqrt{(K_0-2m\alpha_0\bar{n}_0)^2-6m\alpha_0\bar{n}_0w_{\text{eff}}}-(K_0-2m\alpha_0\bar{n}_0)]/(6m\alpha_0\bar{n}_0)$ if $m,\alpha_0,\bar{n}_0\neq 0$, or $q_{\max}^2=-w_{\text{eff}}/(2K_0)$ if one of $m,\alpha_0,\bar{n}_0=0$.

For the heterostructural systems presented below and the parameters chosen, the condition $w_{\text{eff}}>0$ is always satisfied in the bulk phases, keeping homogeneous concentration profile within each layer. Concentration heterogeneity may occur across the system configuration, which however is due to the effect of interfaces or due to composition overshooting, a phenomenon caused by alloy intermixing that will be discussed in detailed below.

B. Results: Equilibrium profiles and layer growth

Equations (88)–(93) were solved numerically using a pseudospectral method and an exponential propagation scheme for time integration of stiff equations [90,91]. Results of the corresponding morphological and compositional 1D profiles are shown in Figs. 1–5, for two types of configurations of liquid-solid-solid and liquid-solid coexistence or growth. For the simulations shown here we choose a time step $\Delta t=1$, which can be made as large as this due to the numerical scheme we used; The numerical grid spacing used is $\Delta y=\lambda_0/8$ (where $\lambda_0=2\pi/q_0$). To emulate a liquid-solid (or liquid-solid-solid) heterostructure and apply periodic boundary conditions in the numerical calculation, the initial configuration is set as two (or four) symmetric interfaces located at $y=L_y/4$ and $3L_y/4$ (or $y=L_y/6$, $L_y/3$, $2L_y/3$, and $5L_y/6$), separating different liquid or solid regions. These interfaces need to be set sufficiently far apart from each other to avoid any interface coupling and the artifacts of finite size effects. For results shown below we choose the 1D system size perpendicular to the interfaces as $L_y=2048\Delta y$, with similar results obtained in calculations up to $L_y=8192\Delta y$. Also, the parameters used in the amplitude equations are based on the phase diagrams given in Ref. [32] showing liquid-solid and solid-solid coexistence, i.e., $(g,g_2,u_0,K_0,v_1)=(-1.8,-0.6,4,1,0)$, $w_0=0.008$ or 0.088, $\alpha_0=0.3$ or 0, and $\epsilon=\pm 0.02$.

1. Liquid-solid and liquid-solid-solid coexistence

The equilibrium profile for a liquid-solid(I)-solid(II) coexistence is given in Fig. 1 (with time corresponding to $t=2\times 10^7$). To obtain the liquid-solid-solid coexistence, we use $\epsilon=0.02$, $\alpha_0=0.3$, and $w_0=0.008$ (from the eutectic phase diagram in Ref. [32]), set the initial length ratio of liquid:solid(I):solid(II) as 1/3:1/3:1/3, and let all of ψ_0^0, A_j^0, and n_0^0 evolve with time until a stationary state is reached. Solid II is treated as a substrate (unstrained), and hence in the amplitude Eqs. (88)–(93) we set $\delta_0=\delta_0^{\text{II}}=-1+\sqrt{1-2\alpha_0\psi_0^{\text{II}}}$. Due to

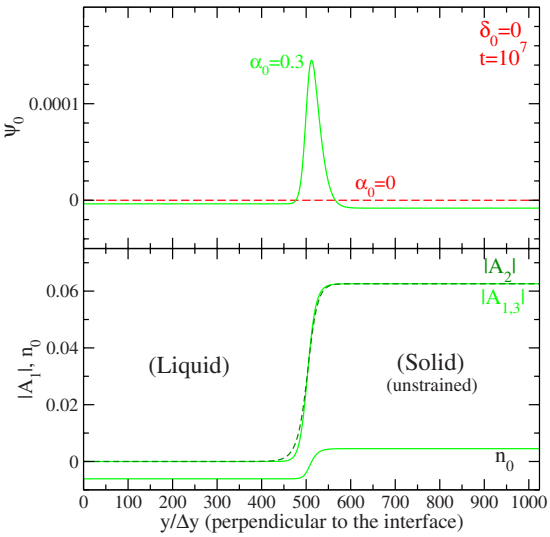

FIG. 3. (Color online) Liquid-solid coexistence profiles for unstrained solid layer (with $\delta_0=0$) and $\alpha_0=0$ and 0.3. The other parameters are the same as Fig. 2. In the lower panel the $|A_j|$ and n_0 profiles overlap for $\alpha_0=0$ and 0.3.

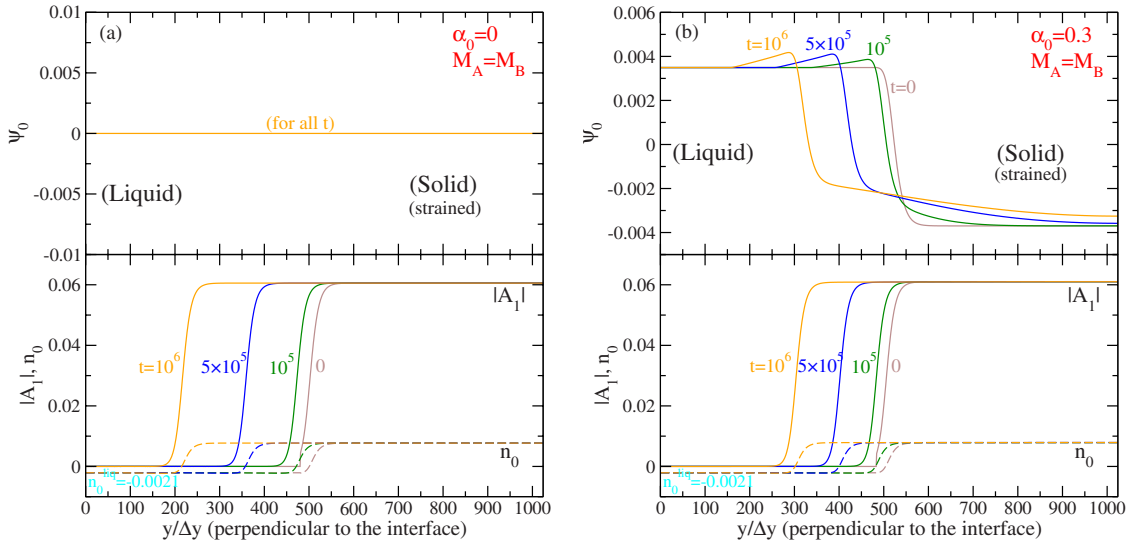

FIG. 4. (Color online) Growth of strained solid layer from a liquid-solid initial configuration, with $\alpha_0=0$ (a) and 0.3 (b) and equal mobility $M_A=M_B$. The parameters are the same as the corresponding liquid-solid coexistence state given in Fig. 2, except for $n_0=-0.0021$ in the liquid region where a constant flux boundary condition is set up.

nonzero solute expansion coefficient α_0, i.e., different atomic sizes of A and B alloy components, solid I is strained (with misfit ε_m with respect to the substrate (solid II) being 14.9% for the parameters of Fig. 1). This is consistent with the numerical results in Fig. 1(b), showing zero phase of amplitudes A_j within unstrained solid II and a linear dependence of phase on position y in the bulk of solid I. For comparison, the magnitude of lattice misfit between III-V or II-VI layers is around 0 to 5% (e.g., $\varepsilon_m=4.2\%$ for Ge/Si and less for $Si_xGe_{1-x}/Si_yGe_{1-y}$), while the lattice mismatch for III-V Nitride heteroepitaxial films or III-V/Si heterostructures could reach 10% or more (e.g., $\varepsilon_m=11.5\%$ for InAs/Si).

For a liquid-solid heterostructural configuration, to determine the coexistence state we choose similar parameters except for $w_0=0.088$, $\epsilon=-0.02$, and initially $\psi_0=0$ in the whole system. This corresponds to the single solid phase region (no solid-solid coexistence, only liquid-solid) in the phase diagram [32]. To make the solid strained, we set $\delta_0=0.05$ as given by an external condition (i.e., a substrate), and thus from Eq. (95) the misfit strain in the solid here is about 5%. The results for $\alpha_0=0$ and 0.3 are given in Figs. 2(a) and 2(b), respectively, including the equilibrium profiles (up to $t=2\times10^7$) and the process of time evolution. As expected, for $\alpha_0=0$ (equal atomic size of alloy components) the concentration field ψ_0 remains at 0 all the time, as seen in Fig. 2(a). However, for $\alpha_0=0.3$ the initial $\psi_0=0$ profile splits at the liquid-solid interface [see Fig. 2(b)]. For the parameters used here, $\alpha_0>0$ (with size of atom A larger than that of atom B) and misfit $\varepsilon_m>0$ (compressed solid), and thus the solid would prefer to have more smaller atoms B (with $\psi_0<0$),

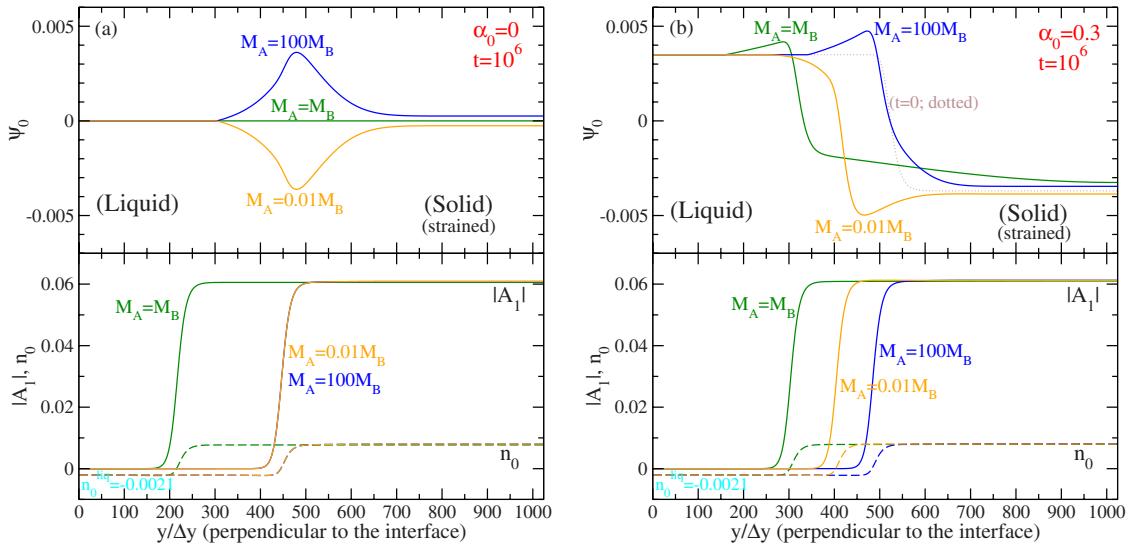

FIG. 5. (Color online) Growth of strained solid layer from a liquid-solid initial configuration, with $\alpha_0=0$ (a) and 0.3 (b), mobilities $M_A=M_B$, $M_A=100M_B$, and $M_A=M_B/100$, and time $t=10^6$. Other parameters are the same as those in Fig. 4. In (a) the $|A_j|$ and n_0 profiles for $M_A=100M_B$ and $M_A=M_B/100$ overlap.

leading to a "dip" on the solid side of the compositional interface; due to the conservation law on the field ψ_0, a "bump" of $\psi_0>0$ (more larger atoms A) appears on the other side via layer interdiffusion or alloy intermixing. As a result of atomic diffusion, such "dip" and "bump" will spread out into the bulk phases as time increases, leading to a positive/negative ψ_0 equilibrium profile of liquid-solid coexistence, as shown in Fig. 2(b).

It is interesting to note that the nonhomogeneous compositional profile can also be found in liquid-solid heterostructures with nonzero α_0 and no misfit strain (i.e., $\delta_0=0$, $\psi_0=0$, and $\alpha_0=0.3$, as in Fig. 3). A slight enrichment of larger atoms A is observed on the surface of unstrained solid, showing as a "peak" (with $\psi_0 \sim 1.5\times 10^{-4}$) at the compositional interface in Fig. 3. Note that this phenomenon of weak surface segregation persists in the equilibrium or stationary configuration (as tested up to $t=10^7$), and is caused by unequal atomic sizes of alloy components. Due to the conservation of the ψ_0 field and the appearance of concentration "peak" at interface, the bulk values of concentration field ψ_0 in both liquid and solid regions deviate from the 0 value in the corresponding phase diagram, as mediated by the alloy diffusion process. We find that this deviation is a result of finite size effect: the deviation decreases with increasing system size, as confirmed in our simulations of $L_y=1024\Delta y$, $2048\Delta y$, and $8192\Delta y$. Thus in the thermodynamic limit (with $L_y\to\infty$) $\psi_0=0$ is expected in the liquid and solid bulks, consistent with the equilibrium phase diagram for unstrained systems. On the other hand, the effect of surface enrichment would be preserved, as we have observed in simulations of various system sizes.

2. Coherent strained layer growth and front motion

To simulate the process of strained layer growth encountered in most experiments, we start from a liquid-solid(strained) coexisting configuration and let the liquid solidify, leading to a growing front of the strained solid layer (as shown in Fig. 4). The initial condition is set as the liquid-solid coexistence profiles given in Fig. 2, with only n_0 in liquid changed to $n_0^{\mathrm{liq}}=-0.0021$ to initialize the solidification and growth while all others (including concentration ψ_0 and amplitudes A_j) being kept the same as the coexistence condition. The growth rate of the strained layer can be controlled by the setting of liquid n_0^{liq}, i.e., its deviation from the equilibrium or coexistence value. A boundary condition of constant flux is kept in the liquid region (with distance $100\Delta y$ beyond the moving interface).

The growth process is shown in Fig. 4, for equal mobility $M_A=M_B$, 5% misfit strain for solid layer, and up to $t=10^6$. The liquid-solid front moves smoothly for both $\alpha_0=0$ and 0.3, as seen from the amplitude and n_0 profiles in the figure. For $\alpha_0=0$, the concentration ψ_0 in both liquid and solid layers remains uniform at the initial value 0, as in the equilibrium state. However, the results for $\alpha_0=0.3$ show a phenomenon of composition overshooting at the growth front of strained solid [see Fig. 4(b)]. Such overshooting effect reveals as the increase of ψ_0 (i.e., more A or less B atoms) around the interface, resulting in the phenomenon of surface enrichment: The A atoms (with larger atomic size for $\alpha_0>0$) are segregated on the solid surface with compressive strain. As time increases, such variation of alloy concentration will propagate into the bulk of solid layer as a result of atomic diffusion (note that the concentration of liquid bulk remains unchanged due to the constant flux boundary condition).

Figure 5 shows that the mobility disparity between different alloy components plays an important role on this overshooting effect. Atoms with larger mobility will accumulate on the surface, even with $\alpha_0=0$. As seen in the concentration profile of Fig. 5(a), a peak of larger (or smaller) ψ_0 appears around the liquid-solid interface for $M_A>M_B$ (or $M_A<M_B$), while no overshooting is observed in the case of equal mobility. For nonzero α_0 [Fig. 5(b)], the effect of surface enrichment of A atoms will be enhanced when $M_A>M_B$, while when $M_A<M_B$ the B atom enrichment is observed at large enough time.

Another effect of mobility difference presented in Fig. 5 is the change of solid layer growth rate or front moving speed. For large disparity of atomic mobility between A and B components, one of the components moves much slower compared to the other one and thus would hinder the atomic diffusion process. This leads to a slower motion of interface, as seen in Fig. 5. Thus we can expect that in the limit of $M_A/M_B\gg 1$ (or $M_A/M_B\ll 1$), B (or A) atoms would be almost immobile compared to A (or B) and hence would pin the interface location, resulting in a frozen front. This has been incorporated in the amplitude equations developed above: When $m=\pm 1$ [with $m=(M_A-M_B)/(M_A+M_B)$ as defined in Eq. (32)], Eq. (64) yields $dA_j/dt=0$, a frozen amplitude profile. Furthermore, the concentration profile is symmetric with respect to the sign of m (i.e., $M_A/M_B>1$ vs <1) for $\alpha_0=0$, as shown in Fig. 5(a) for $M_A/M_B=100$ and 10^{-2} which yield the same front moving rate and the same A_j and n_0 profiles. The situation for nonzero α_0 (different atomic sizes) is more complicated. In our calculations of Fig. 5(b) with $\alpha_0=0.3$ and 5% compressive misfit, the liquid-solid coexisting profile yields $\psi_0>0$ (A-rich) in the liquid region and <0 (B-rich) in the solid layer [see also Fig. 2(b)]. When $M_A=100M_B$, the segregation of fast A atoms around the interface would tend to hinder the growth of B-rich solid layer, while for $M_A=M_B/100$ the accumulation of fast B atoms will naturally be accompanied by the expansion of solid region, resulting in a faster solid growth.

The composition overshooting effect presented here and the associated surface enrichment phenomenon can be viewed as a result of interface intermixing process via atomic interdiffusion and mass transport of alloy components, showing as the vertical phase separation or segregation in the liquid-solid interface region. Such process of vertical separation has also been found in 2D simulations of binary PFC equations [25], where the component of greater size or larger mobility was found to accumulate near undulated solid surface in a liquid/substrate epitaxial system. Importantly, the results shown here are consistent with recent experimental observations of surface or interface segregation phenomenon in alloy heterostructures, particularly in semiconductor epitaxial layers. Most experiments focus on III-V or group IV heteroepitaxial films, with typical systems including InGaAs/GaAs(001) (with In enrichment or segregation [66–68]),

Ge(SiGe)/Si(001) (with Ge segregation [69,70]), and multilayers or superlattices of InP/InGaAs (with excess InAs at the interface [71]), GaAs/GaSb (with Sb segregation and Sb-As exchange and intermixing [72]), GaAs/InAs (with In segregation [73]), etc. In these experimental systems the segregation or enrichment effect involves the coupling of various factors of different atomic size (nonzero α_0), misfit strain, and unequal mobility of alloy components (e.g., $M_{\mathrm{Ge}} > M_{\mathrm{Si}}$ and $M_{\mathrm{In}} > M_{\mathrm{Ga}}$), each of which has been identified in our analysis given above.

VI. CONCLUSIONS

In this paper we have furthered the development of the phase-field-crystal methodology by systematically deriving the PFC dynamic model equations from dynamical density functional theory (DDFT) and completing the derivation of the corresponding amplitude equation formalism. A truncation of the DFT free energy functional up to three-point direct correlation functions has been used, and the dynamics derived from DDFT has been further simplified through lowest order approximations via a simple scale analysis to obtain the PFC equations, for both single-component and binary alloy systems. For the binary PFC model, the corresponding amplitude equations (both deterministic and stochastic) have been established via a hybrid multiple-scale approach, which describe large or "slow" scale dynamics of structural and compositional profiles based on the underlying crystalline state. Compared to other recent developments which have mainly focused on the evolution of complex structural amplitudes and concentration field, this work presents results that incorporate the new effects of mobility difference between alloy components, the coupling to zero-mode average atomic density, and also noise dynamics. Although the results of amplitude equations that we derive are for 2D hexagonal crystalline state, they can be extended to 3D bcc or fcc structures by following a procedure similar to the one developed here and adopting the corresponding basic wavevectors (see also Ref. [32]).

This amplitude equation formalism for binary PFC has been applied to identifying the mechanisms and parameter coupling during the process of surface segregation and alloy intermixing. Both liquid-solid and liquid-solid-solid epitaxial heterostructures have been examined, including morphological and compositional profiles. We find that the effect of concentration segregation on solid surface is controlled by material parameters such as the disparity of atomic size and mobility between different alloy components and misfit strain in solid layers. In the cases of nonzero solute expansion coefficient or unequal atomic mobility, an effect of composition overshooting around liquid-solid interface is obtained during strained layer growth, corresponding to vertical phase separation or segregation in the interface region. These results are consistent with recent experimental findings in heteroepitaxial systems, particularly the phenomenon of surface or interface segregation showing as the enrichment of one of the alloy species as compared to the bulk phase. This sample application of the amplitude equation formalism developed here has further illustrated the features and advantages of the PFC methodology, particularly in terms of modeling and understanding complex material phenomena involving spacial and temporal scales of experimental relevance.

ACKNOWLEDGMENTS

Z.-F.H. acknowledges support from the National Science Foundation (NSF) under Grant No. CAREER DMR-0845264. K.R.E. acknowledges support from NSF under Grant No. DMR-0906676. N.P. acknowledges support from the National Science and Engineering Research Council of Canada.

APPENDIX A: ALTERNATIVE DERIVATIONS OF BINARY PFC DYNAMICS VIA DDFT

1. Alternative derivation I

In the following we provide an alternative derivation procedure for PFC dynamics, including two steps: (i) directly use the original free energy functional (17) and the DDFT Eqs. (15) to obtain the expressions of $\partial\rho_{A(B)}/\partial t$, and then (ii) derive the dynamics of n and ψ through Eq. (25), instead of using Eqs. (21) and (28) as in Sec. II B.

Define $n_A=(\rho_A-\rho_l^A)/\rho_l$ and $n_B=(\rho_B-\rho_l^B)/\rho_l$, and hence the free energy functional (17) can be rewritten as [using the expansion (18)]

$$\begin{aligned}\Delta\mathcal{F}/\rho_l k_B T = \int d\boldsymbol{r}\Bigg\{ & \Delta\rho_l^A\left(1+\frac{n_A}{\Delta\rho_l^A}\right)\ln\left(1+\frac{n_A}{\Delta\rho_l^A}\right) \\ & + \Delta\rho_l^B\left(1+\frac{n_B}{\Delta\rho_l^B}\right)\ln\left(1+\frac{n_B}{\Delta\rho_l^B}\right) - (n_A+n_B) \\ & + \frac{\rho_l}{2}[n_A(\hat{C}_2^{AA}\nabla^2+\hat{C}_4^{AA}\nabla^4)n_A + n_B(\hat{C}_2^{BB}\nabla^2 \\ & + \hat{C}_4^{BB}\nabla^4)n_B + 2n_A(\hat{C}_2^{AB}\nabla^2+\hat{C}_4^{AB}\nabla^4)n_B + \hat{C}_0^{AA}n_A^2 \\ & + \hat{C}_0^{BB}n_B^2 + 2\hat{C}_0^{AB}n_A n_B] + \frac{\rho_l^2}{6}[\hat{C}_0^{AAA}n_A^3 + \hat{C}_0^{BBB}n_B^3 \\ & + 3\hat{C}_0^{AAB}n_A^2 n_B + 3\hat{C}_0^{ABB}n_A n_B^2]\Bigg\}, \end{aligned} \tag{A1}$$

where $\Delta\rho_l^A=\rho_l^A/\rho_l$ and $\Delta\rho_l^B=\rho_l^B/\rho_l$. From the DDFT Eqs. (15) we can obtain the PFC equations for A & B components respectively, i.e.,

$$\begin{aligned}\partial n_A/\partial t = M_A k_B T\Bigg\{ & \nabla^2\Bigg[(1+\rho_l^A\hat{C}_0^{AA})n_A + \rho_l^A(\hat{C}_2^{AA}\nabla^2+\hat{C}_4^{AA}\nabla^4)n_A \\ & + \frac{1}{3}\rho_l^2\hat{C}_0^{AAA}n_A^3 + \frac{\rho_l}{2}(\hat{C}_0^{AA}+\rho_l^A\hat{C}_0^{AAA})n_A^2\Bigg] \\ & + \rho_l\nabla\cdot[n_A(\hat{C}_2^{AA}\nabla^2+\hat{C}_4^{AA}\nabla^4)\nabla n_A] \\ & + \rho_l\nabla\cdot\Bigg[(n_A+\Delta\rho_l^A)\nabla\Bigg[(\hat{C}_0^{AB}+\hat{C}_2^{AB}\nabla^2+\hat{C}_4^{AB}\nabla^4)n_B\end{aligned}$$

$$+\frac{\rho_l}{2}(2\hat{C}_0^{AAB}n_An_B+\hat{C}_0^{ABB}n_B^2)\Big]\Big]\Big\}, \quad \text{(A2)}$$

$$\partial n_B/\partial t = M_Bk_BT\Big\{\nabla^2\Big[(1+\rho_l^B\hat{C}_0^{BB})n_B+\rho_l^B(\hat{C}_2^{BB}\nabla^2+\hat{C}_4^{BB}\nabla^4)n_B + \frac{1}{3}\rho_l^2\hat{C}_0^{BBB}n_B^3+\frac{\rho_l}{2}(\hat{C}_0^{BB}+\rho_l^B\hat{C}_0^{BBB})n_B^2\Big] + \rho_l\nabla\cdot[n_B(\hat{C}_2^{BB}\nabla^2+\hat{C}_4^{BB}\nabla^4)\nabla n_B] + \rho_l\nabla\cdot\Big[(n_B+\Delta\rho_l^B)\nabla\Big[(\hat{C}_0^{AB}+\hat{C}_2^{AB}\nabla^2+\hat{C}_4^{AB}\nabla^4)n_A + \frac{\rho_l}{2}(2\hat{C}_0^{ABB}n_An_B+\hat{C}_0^{AAB}n_A^2)\Big]\Big]\Big\}. \quad \text{(A3)}$$

Note that $n=n_A+n_B$ and $\psi=[(\rho_l^A-\rho_l^B)+\rho_l(n_A-n_B)]/[\rho_l(1+n)]$, and hence equivalent to Eq. (25) we have

$$\frac{\partial n}{\partial t}=\frac{\partial n_A}{\partial t}+\frac{\partial n_B}{\partial t}, \quad \frac{\partial\psi}{\partial t}=\frac{1}{1+n}\Big[(1-\psi)\frac{\partial n_A}{\partial t}-(1+\psi)\frac{\partial n_B}{\partial t}\Big]. \quad \text{(A4)}$$

Substituting Eqs. (A2) and (A3) into Eq. (A4), and noting $n_A=(1+n)(1+\psi)/2-\Delta\rho_l^A$, $n_B=(1+n)(1-\psi)/2-\Delta\rho_l^B$, $M_A=\rho_l(M_1+M_2)$, and $M_B=\rho_l(M_1-M_2)$, we can derive the binary PFC equations for n and ψ, which are exactly the same as Eqs. (26), (29), and (30).

2. Alternative derivation II

Another alternative derivation for PFC dynamics is to start with Eqs. (26)–(28) as already derived in Sec. II B. Different from Sec. II B, in the formula (28) for $\mathcal{D}_1$ and $\mathcal{D}_2$ if considering that the chemical potentials $\mu_n=\delta\mathcal{F}/\delta n$ and $\mu_N=\delta\mathcal{F}/\delta\psi$ are slowly varying quantities and retaining terms up to the lowest order, we have

$$\mathcal{D}_1\simeq\nabla^2\frac{\delta\mathcal{F}}{\delta n}, \quad \mathcal{D}_2\simeq\nabla^2\frac{\delta\mathcal{F}}{\delta\psi}, \quad \text{(A5)}$$

as used in the original PFC model [25,32]. As in the previous work, the logarithm terms in the free energy functional (21) are expanded in a power series, yielding (up to 4th order of n and ψ)

$$\Delta\mathcal{F}/\rho_lk_BT=\int d\boldsymbol{r}\Big\{\Big[\frac{1}{2}\psi^2+\beta(\psi)\Big]n+\frac{1}{2}B^\ell(\psi)n^2 + \frac{1}{3}(\tau+\tilde{B}_1\psi)n^3+\frac{1}{4}vn^4+\frac{1}{2}w\psi^2+\frac{1}{3}\beta_3\psi^3+\frac{1}{4}u\psi^4 + \frac{1}{2}(1+n)(2B^xR^2\nabla^2+B^xR^4\nabla^4)n + \frac{1}{2}K|\nabla[(1+n)\psi]|^2+\frac{\kappa}{2}(\nabla^2[(1+n)\psi])^2\Big\}, \quad \text{(A6)}$$

where $\tau=\tilde{B}_0-1/2$, $w=1+\beta_2$, $v=u=1/3$, and other parameters (such as B^ℓ, β, K, and κ) are defined in Eq. (22).

Substituting Eq. (A6) into Eq. (A5), we find (up to third order)

$$\mathcal{D}_1=\nabla^2\Big\{-(B_0^x-B_0^\ell)n+B_0^x(R_0^2\nabla^2+1)^2n+(B_1^\ell\psi+B_2^\ell\psi^2)n + (\tau+\tilde{B}_1\psi)n^2+vn^3+\beta_0\psi+\Big(\frac{1}{2}+\beta_1\Big)\psi^2+\beta_3\psi^3 + \psi(-K\nabla^2+\kappa\nabla^4)[(1+n)\psi]+B_0^x\Big(\alpha_2R_0^2\nabla^2+\frac{\alpha_4}{2}R_0^4\nabla^4\Big) \times[(1+n)\psi]+B_0^x\psi\Big(\alpha_2R_0^2\nabla^2+\frac{\alpha_4}{2}R_0^4\nabla^4\Big)n\Big\}, \quad \text{(A7)}$$

$$\mathcal{D}_2=\nabla^2\Big\{\beta_0n+B_0^x(1+n)\Big(\alpha_2R_0^2\nabla^2+\frac{\alpha_4}{2}R_0^4\nabla^4\Big)n + [(1+2\beta_1)\psi+3\beta_3\psi^2]n+\frac{1}{2}(B_1^\ell+2B_2^\ell\psi)n^2+\frac{1}{3}\tilde{B}_1n^3 + w\psi+\beta_3\psi^2+u\psi^3+(1+n)(-K\nabla^2+\kappa\nabla^4)[(1+n)\psi]\Big\}. \quad \text{(A8)}$$

As in Sec. II B, we can rescale the PFC equations (using the same length and time scales as well as the scales for n and ψ fields). Following the scale analysis discussed at the end of Sec. II B, to lowest order approximation we can obtain the same simplified binary PFC equations given in Eqs. (38) and (39), albeit with different forms of rescaled parameters $g_2=g_0\tau/B_0^x$ and $v_1=g_0(1/2+\beta_1)/B_0^x$ (other parameters g, w_0, α_0, and g_0 are the same as those defined in Sec. II B but with different value of v).

[1] P. Politi, G. Grenet, A. Marty, A. Ponchet, and J. Villain, Phys. Rep. **324**, 271 (2000).

[2] J. Stangl, V. Holy, and G. Bauer, Rev. Mod. Phys. **76**, 725 (2004).

[3] Z.-F. Huang and K. R. Elder, Phys. Rev. Lett. **101**, 158701 (2008).

[4] J. D. Gunton, M. San Miguel, and P. S. Sahni, *Kinetics of First Order Phase Transitions*, Phase Transitions and Critical Phenomena Vol. 8 (Academic, London, 1983).

[5] J. E. Guyer and P. W. Voorhees, Phys. Rev. Lett. **74**, 4031 (1995).

[6] G. Nandipati and J. G. Amar, Phys. Rev. B **73**, 045409 (2006).

[7] M. T. Lung, C. H. Lam, and L. M. Sander, Phys. Rev. Lett. **95**, 086102 (2005).

[8] A. Baskaran, J. Devita, and P. Smereka, Continuum Mech. Thermodyn. **22**, 1 (2010).

[9] D. Wolf, V. Yamakov, S. R. Phillpot, A. K. Mukherjee, and H. Gleiter, Acta Mater. **53**, 1 (2005).
[10] P. M. Derlet, P. Gumbsch, R. Hoagland, J. Li, D. L. McDowell, H. Van Swygenhoven, and J. Wang, MRS Bull. **34**, 184 (2009).
[11] B. J. Spencer, P. W. Voorhees, and S. H. Davis, Phys. Rev. Lett. **67**, 3696 (1991).
[12] Z.-F. Huang and R. C. Desai, Phys. Rev. B **65**, 205419 (2002).
[13] Z.-F. Huang and R. C. Desai, Phys. Rev. B **65**, 195421 (2002).
[14] Z.-F. Huang and R. C. Desai, Phys. Rev. B **67**, 075416 (2003).
[15] Z.-F. Huang, D. Kandel, and R. C. Desai, Appl. Phys. Lett. **82**, 4705 (2003).
[16] Y. Tu and J. Tersoff, Phys. Rev. Lett. **98**, 096103 (2007).
[17] R. C. Desai, H. K. Kim, A. Chatterji, D. Ngai, S. Chen, and N. Yang, Phys. Rev. B **81**, 235301 (2010).
[18] K. R. Elder, F. Drolet, J. M. Kosterlitz, and M. Grant, Phys. Rev. Lett. **72**, 677 (1994).
[19] K. R. Elder, M. Grant, N. Provatas, and J. M. Kosterlitz, Phys. Rev. E **64**, 021604 (2001).
[20] K. Kassner, C. Misbah, J. Müller, J. Kappey, and P. Kohlert, Phys. Rev. E **63**, 036117 (2001).
[21] B. Echebarria, R. Folch, A. Karma, and M. Plapp, Phys. Rev. E **70**, 061604 (2004).
[22] L. Gránásy, T. Pusztai, T. Börzsönyi, G. Tóth, G. Tegze, J. A. Warren, and J. F. Douglas, J. Mater. Res. **21**, 309 (2006).
[23] K. R. Elder, M. Katakowski, M. Haataja, and M. Grant, Phys. Rev. Lett. **88**, 245701 (2002).
[24] K. R. Elder and M. Grant, Phys. Rev. E **70**, 051605 (2004).
[25] K. R. Elder, N. Provatas, J. Berry, P. Stefanovic, and M. Grant, Phys. Rev. B **75**, 064107 (2007).
[26] N. Goldenfeld, B. P. Athreya, and J. A. Dantzig, Phys. Rev. E **72**, 020601(R) (2005).
[27] B. P. Athreya, N. Goldenfeld, and J. A. Dantzig, Phys. Rev. E **74**, 011601 (2006).
[28] B. P. Athreya, N. Goldenfeld, J. A. Dantzig, M. Greenwood, and N. Provatas, Phys. Rev. E **76**, 056706 (2007).
[29] P. Y. Chan and N. Goldenfeld, Phys. Rev. E **80**, 065105 (2009).
[30] D. H. Yeon, Z.-F. Huang, K. R. Elder, and K. Thornton, Philos. Mag. **90**, 237 (2010).
[31] K. R. Elder, J. Berry, and N. Provatas, TMS Lett. **3**, 41 (2004).
[32] K. R. Elder, Z.-F. Huang, and N. Provatas, Phys. Rev. E **81**, 011602 (2010).
[33] S. van Teeffelen, R. Backofen, A. Voigt, and H. Löwen, Phys. Rev. E **79**, 051404 (2009).
[34] R. Backofen, A. Ratz, and A. Voigt, Philos. Mag. Lett. **87**, 813 (2007).
[35] G. Tegze, L. Granásy, G. I. Toth, F. Podmaniczky, A. Jaatinen, T. Ala-Nissila, and T. Pusztai, Phys. Rev. Lett. **103**, 035702 (2009).
[36] K.-A. Wu and P. W. Voorhees, Phys. Rev. B **80**, 125408 (2009).
[37] Z.-F. Huang and K. R. Elder, Phys. Rev. B **81**, 165421 (2010).
[38] K.-A. Wu and A. Karma, Phys. Rev. B **76**, 184107 (2007).
[39] S. Majaniemi and N. Provatas, Phys. Rev. E **79**, 011607 (2009).
[40] J. Berry, M. Grant, and K. R. Elder, Phys. Rev. E **73**, 031609 (2006).
[41] J. Berry, K. R. Elder, and M. Grant, Phys. Rev. B **77**, 224114 (2008).
[42] J. Mellenthin, A. Karma, and M. Plapp, Phys. Rev. B **78**, 184110 (2008).
[43] R. Spatschek and A. Karma, Phys. Rev. B **81**, 214201 (2010).
[44] C. V. Achim, M. Karttunen, K. R. Elder, E. Granato, T. Ala-Nissila, and S. C. Ying, Phys. Rev. E **74**, 021104 (2006).
[45] J. A. P. Ramos, E. Granato, C. V. Achim, S. C. Ying, K. R. Elder, and T. Ala-Nissila, Phys. Rev. E **78**, 031109 (2008).
[46] C. V. Achim, J. A. P. Ramos, M. Karttunen, K. R. Elder, E. Granato, T. Ala-Nissila, and S. C. Ying, Phys. Rev. E **79**, 011606 (2009).
[47] J. A. P. Ramos, E. Granato, S. C. Ying, C. V. Achim, K. R. Elder, and T. Ala-Nissila, Phys. Rev. E **81**, 011121 (2010).
[48] J. Berry, K. R. Elder, and M. Grant, Phys. Rev. E **77**, 061506 (2008).
[49] P. Stefanovic, M. Haataja, and N. Provatas, Phys. Rev. Lett. **96**, 225504 (2006).
[50] P. Stefanovic, M. Haataja, and N. Provatas, Phys. Rev. E **80**, 046107 (2009).
[51] M. Cheng and J. A. Warren, J. Comput. Phys. **227**, 6241 (2008).
[52] T. Hirouchi, T. Takaki, and Y. Tomita, Comput. Mater. Sci. **44**, 1192 (2009).
[53] G. Tegze, G. Bansel, G. I. Toth, T. Pusztai, Z. Y. Fan, and L. Granásy, J. Comput. Phys. **228**, 1612 (2009).
[54] S. Majaniemi and M. Grant, Phys. Rev. B **75**, 054301 (2007).
[55] S. Majaniemi, M. Nonomura, and M. Grant, Eur. Phys. J. B **66**, 329 (2008).
[56] A. Jaatinen, C. V. Achim, K. R. Elder, and T. Ala-Nissila, Phys. Rev. E **80**, 031602 (2009).
[57] T. V. Ramakrishnan and M. Yussouff, Phys. Rev. B **19**, 2775 (1979).
[58] A. D. J. Haymet and D. W. Oxtoby, J. Chem. Phys. **74**, 2559 (1981).
[59] S. W. Rick and A. D. J. Haymet, J. Phys. Chem. **94**, 5212 (1990).
[60] A. R. Denton and N. W. Ashcroft, Phys. Rev. A **42**, 7312 (1990).
[61] Y. Singh, Phys. Rep. **207**, 351 (1991).
[62] H. Löwen, Phys. Rep. **237**, 249 (1994).
[63] Y. M. Jin and A. G. Khachaturyan, J. Appl. Phys. **100**, 013519 (2006).
[64] A. D. J. Haymet, J. Chem. Phys. **78**, 4641 (1983).
[65] W. A. Curtin, J. Chem. Phys. **88**, 7050 (1988).
[66] J. M. Moison, C. Guille, F. Houzay, F. Barthe, and M. Van Rompay, Phys. Rev. B **40**, 6149 (1989).
[67] T. Walther, A. G. Cullis, D. J. Norris, and M. Hopkinson, Phys. Rev. Lett. **86**, 2381 (2001).
[68] J. G. Cederberg, J. Cryst. Growth **307**, 44 (2007).
[69] T. Walther, C. J. Humphreys, and A. G. Cullis, Appl. Phys. Lett. **71**, 809 (1997).
[70] U. Denker, A. Rastelli, M. Stoffel, J. Tersoff, G. Katsaros, G. Costantini, K. Kern, N. Y. Jin-Phillip, D. E. Jesson, and O. G. Schmidt, Phys. Rev. Lett. **94**, 216103 (2005).
[71] M. Gerling, A. Gustafsson, D. H. Rich, D. Ritter, and D. Gershoni, Appl. Phys. Lett. **78**, 1370 (2001).
[72] C. Dorin, J. Mirecki Millunchick, and C. Wauchope, J. Appl. Phys. **94**, 1667 (2003).
[73] C. Pearson, C. Dorin, J. M. Millunchick, and B. G. Orr, Phys. Rev. Lett. **92**, 056101 (2004).
[74] R. Evans, Adv. Phys. **28**, 143 (1979).

[75] W. Dieterich, H. L. Frisch, and A. Majhofer, Z. Phys. B **78**, 317 (1990).
[76] U. M. B. Marconi and P. Tarazona, J. Chem. Phys. **110**, 8032 (1999).
[77] A. J. Archer and R. Evans, J. Chem. Phys. **121**, 4246 (2004).
[78] U. M. B. Marconi, P. Tarazona, F. Cecconi, and S. Melchionna, J. Phys.: Condens. Matter **20**, 494233 (2008).
[79] Garnet Kin-Lic Chan and R. Finken, Phys. Rev. Lett. **94**, 183001 (2005).
[80] A. J. Archer, J. Phys.: Condens. Matter **17**, 1405 (2005).
[81] S. J. Smithline and A. D. J. Haymet, J. Chem. Phys. **86**, 6486 (1987).
[82] S. W. Rick and A. D. J. Haymet, J. Chem. Phys. **90**, 1188 (1989).
[83] S. Zhou and E. Ruckenstein, Phys. Rev. E **61**, 2704 (2000).
[84] For the ideal-gas part $(1+n)\ln(1+n)$ in the free energy [Eq. (5)], it contributes to a term $\nabla^2 n$ in the dynamics $\mathbf{\nabla}\cdot[(1+n)\mathbf{\nabla}\,\delta\mathcal{F}/\delta n]$ of Eq. (7). It is straightforward to show that this can also be obtained via first expanding $(1+n)\ln(1+n)=n+n^2/2-n^3/6+n^4/12-\cdots$ as a power series of n, similar to the previous work of original PFC model [25,56] but without truncating at any given order, and then substituting into the functional derivative.
[85] M. C. Cross and P. C. Hohenberg, Rev. Mod. Phys. **65**, 851 (1993).
[86] P. C. Matthews and S. M. Cox, Nonlinearity **13**, 1293 (2000).
[87] A. J. Archer and M. Rauscher, J. Phys. A **37**, 9325 (2004).
[88] R. Graham, Phys. Rev. A **10**, 1762 (1974).
[89] P. C. Hohenberg and J. B. Swift, Phys. Rev. A **46**, 4773 (1992).
[90] R. A. Friesner, L. S. Tuckerman, B. C. Dornblaser, and T. V. Russo, J. Sci. Comput. **4**, 327 (1989).
[91] M. C. Cross, D. I. Meiron, and Y. Tu, Chaos **4**, 607 (1994).